

# Two distinct halo populations in the solar neighborhood. II. ★,★★

## Evidence from stellar abundances of Mn, Cu, Zn, Y, and Ba.

P.E. Nissen<sup>1</sup> and W.J. Schuster<sup>2</sup>

<sup>1</sup> Department of Physics and Astronomy, University of Aarhus, DK-8000 Aarhus C, Denmark. e-mail: pen@phys.au.dk

<sup>2</sup> Observatorio Astronómico Nacional, Universidad Nacional Autónoma de México, Apartado Postal 877, C.P. 22800 Ensenada, B.C., México. e-mail: schuster@astro.unam.mx

Received 1 February 2011 / Accepted 16 March 2011

### ABSTRACT

**Context.** Current models of galaxy formation predict that the Galactic halo was assembled hierarchically. By measuring abundance ratios in stars it may be possible to identify substructures in the halo resulting from this process.

**Aims.** A previous study of 94 dwarf stars with  $-1.6 < [\text{Fe}/\text{H}] < -0.4$  in the solar neighborhood has revealed the existence of two distinct halo populations with a systematic difference in  $[\alpha/\text{Fe}]$  at a given metallicity. In continuation of that work, abundances of Mn, Cu, Zn, Y, and Ba are determined for the same sample of stars.

**Methods.** Equivalent widths of atomic lines are measured from high resolution VLT/UVES and NOT/FIES spectra and used to derive abundance ratios from an LTE analysis based on MARCS model atmospheres. The analysis is made relative to two thick-disk stars, HD 22879 and HD 76932, such that very precise differential values are obtained.

**Results.** Systematic differences between the ‘high- $\alpha$ ’ and ‘low- $\alpha$ ’ halo populations are found for  $[\text{Cu}/\text{Fe}]$ ,  $[\text{Zn}/\text{Fe}]$ , and  $[\text{Ba}/\text{Y}]$ , whereas there is no significant difference in the case of  $[\text{Mn}/\text{Fe}]$ . At a given metallicity,  $[\text{Cu}/\text{Fe}]$  shows a large scatter that is closely correlated with a corresponding scatter in  $[\text{Na}/\text{Fe}]$  and  $[\text{Ni}/\text{Fe}]$ .

**Conclusions.** The metallicity trends of  $[\text{Cu}/\text{Fe}]$ ,  $[\text{Zn}/\text{Fe}]$ , and  $[\text{Ba}/\text{Y}]$  can be explained from existing nucleosynthesis calculations if the high- $\alpha$  stars formed in regions with such a high star formation rate that only massive stars and Type II supernovae contributed to the chemical enrichment. The low- $\alpha$  stars, on the other hand, most likely originate from systems with a slower chemical evolution, characterized by additional enrichment from Type Ia supernovae and low-mass AGB stars.

**Key words.** Stars: atmospheres – Stars: abundances – Galaxy: abundances – Galaxy: halo – Galaxy: formation

### 1. Introduction

According to cosmological  $\Lambda$ CDM simulations, large galaxies such as the Milky Way were formed hierarchically. Evidence of spatial and kinematical substructures in the Galactic halo resulting from this process has indeed been found as reviewed by Helmi (2008) and Klement (2010). Elemental abundance ratios of halo stars may also be used to probe this formation process by so-called ‘chemical tagging’ of the ‘building blocks’ (Freeman & Bland-Hawthorn 2002). The F, G, and K stars are of particular interest in this connection, because their atmospheric composition are likely to provide a ‘fossil’ record of the composition of the gas from which the stars once were formed. As found by Korn et al. (2007) from a comparison of dwarf and giant stars in the globular cluster NGC 6397, the atmospheric abundances of heavy elements like Mg, Ca, Ti, and Fe in old dwarf stars may be somewhat decreased by diffusion processes, but the ratios between these elements are practically unchanged.

\* Based on observations made with the Nordic Optical Telescope on La Palma, and on data from the European Southern Observatory ESO/ST-ECF Science Archive Facility (programs 65.L-0507, 67.D-0086, 67.D-0439, 68.D-0094, 68.B-0475, 69.D-0679, 70.D-0474, 71.B-0529, 72.B-0585, 76.B-0133 and 77.B-0507).

\*\* Tables 1, 2, and part of Table 3 are provided as on-line material and are also available at the CDS via anonymous ftp to cdsarc.u-strasbg.fr (130.79.128.5a) or via <http://cdsarc.u-strasbg.fr/viz-bin/qcat?A+A/XXX/xxx>. The complete Table 3 is available in electronic form at the CDS.

Most high-precision studies of abundance ratios in stars are limited to the solar region of the Galaxy. This means that halo stars must be identified by their kinematics, e.g. by having space velocities with respect to the local standard of rest (LSR) well above the characteristic velocities of thin and thick-disk stars. Several such studies have focused on possible correlations between kinematics and  $[\alpha/\text{Fe}]$ , where  $\alpha$  refers to the abundance of  $\alpha$ -capture elements like Mg, Si, Ca and Ti. Fulbright (2002) finds evidence that stars with high values of the total space velocity relative to the LSR,  $V_{\text{total}} > 300 \text{ km s}^{-1}$ , tend to have lower values of  $[\alpha/\text{Fe}]$  than stars with  $150 < V_{\text{total}} < 300 \text{ km s}^{-1}$ . Stephens & Boesgaard (2002) show that  $[\alpha/\text{Fe}]$  is correlated with the apogalactic orbital distance ( $R_{\text{apo}}$ ) in the sense that the outermost stars have the lowest values of  $[\alpha/\text{Fe}]$ . Gratton et al. (2003) divided their sample into two populations according to kinematics: *i*) a ‘dissipative’ component, which comprises thick-disk stars and prograde-rotating halo stars, and *ii*) an ‘accretion’ component consisting of retrograde-rotating halo stars. The accretion component has lower values and a larger scatter for  $[\alpha/\text{Fe}]$  than the dissipative component. This has been confirmed by Jonsell et al. (2005). Furthermore, a recent study of Ishigaki et al. (2010) shows that in the metallicity range  $-2 < [\text{Fe}/\text{H}] < -1$ , the  $[\text{Mg}/\text{Fe}]$  ratio for stars reaching a maximum vertical distance  $Z_{\text{max}} > 5 \text{ kpc}$  above or below the Galactic plane in their orbits tend to be about 0.1 dex lower than  $[\text{Mg}/\text{Fe}]$  for stars with  $Z_{\text{max}} < 5 \text{ kpc}$ .

The  $\alpha$ -elements are mainly produced during Type II supernovae (SNe II) explosions of massive stars on a relatively short time scale,  $\sim 10^7$  years, whereas iron is also produced by Type Ia SNe (SNe Ia) on a longer time scale, i.e. from about  $10^8$  to more than  $10^9$  years (Maoz et al. 2010). The differences in  $[\alpha/\text{Fe}]$  may therefore be explained in terms of differences in the star formation rate (SFR). The outer halo stars may originate from regions characterized by a relatively slow SFR with both SNe Ia and SNe II contributing to the chemical evolution, whereas the inner stars come from regions with such a fast chemical evolution that only SNe II have contributed. Differences in the initial mass function may, however, also play a role, because low-mass SNe II produce lower values of  $[\alpha/\text{Fe}]$  than high-mass SNe II (e.g. Kobayashi et al. 2006).

It is unclear from the works cited above if there is a dichotomy in the distribution of  $[\alpha/\text{Fe}]$  or a more continuous change in  $[\alpha/\text{Fe}]$  as a function of  $R_{\text{apo}}$  or  $Z_{\text{max}}$ . In a recent study, the authors of the present paper (Nissen & Schuster 2010, hereafter NS10) have, however, found evidence for the existence of two distinct halo populations in the solar neighborhood. Abundances were determined for a sample of 94 dwarf and subgiant stars with halo or thick-disk kinematics selected from Strömgren photometry (Schuster et al. 2006) to have metallicities  $-1.6 < [\text{Fe}/\text{H}] < -0.4$  and to lie in a fairly narrow temperature range,  $5200 < T_{\text{eff}} < 6300$  K. A differential abundance analysis of high-resolution spectra enabled us to determine  $[\alpha/\text{Fe}]^1$  with a precision of about 0.02 dex. As seen from Fig. 1 of NS10, the halo stars are distributed into two groups clearly separated in  $[\alpha/\text{Fe}]$  for the metallicity range  $-1.4 < [\text{Fe}/\text{H}] < -0.7$ , i.e. ‘high- $\alpha$ ’ stars having  $[\alpha/\text{Fe}]$  close to 0.30 dex, similar to thick-disk stars, and ‘low- $\alpha$ ’ stars with  $[\alpha/\text{Fe}]$  decreasing from 0.25 dex at  $[\text{Fe}/\text{H}] = -1.4$  to 0.10 dex at  $[\text{Fe}/\text{H}] = -0.7$ . Differences in  $[\text{Na}/\text{Fe}]$  and  $[\text{Ni}/\text{Fe}]$  are also present with a remarkably tight correlation between these two ratios.  $[\text{Cr}/\text{Fe}]$ , on the other hand, is the same for the two populations.

The halo stars in the NS10 sample were selected to have  $V_{\text{total}} > 180 \text{ km s}^{-1}$ . Yet, the high- and low- $\alpha$  populations have different kinematical properties as seen from Fig. 3 in NS10. The high- $\alpha$  stars tend to move on prograde Galactic orbits, whereas two-thirds of the low- $\alpha$  stars have retrograde orbits with an average Galactic rotational velocity component,  $V_{\text{LSR}} \approx -260 \text{ km s}^{-1}$ , close to that of the  $\omega$  Cen globular cluster (Dinescu et al. 1999). Furthermore, the low- $\alpha$  stars have a very wide distribution of the radial velocity component,  $U$ , but comparatively small values of the  $W$  component. All together, this suggests that the low- $\alpha$  stars have been accreted from satellite galaxies including the progenitor galaxy of  $\omega$  Cen (Bekki & Freeman 2003). The high- $\alpha$  stars, on the other hand, are more likely to be formed ‘in situ’ in the Galactic bulge or disk, and then ‘heated’ to halo kinematics by the merging satellites, as suggested from numerical simulations (Zolotov et al. 2009, 2010; Purcell et al. 2010; Qu et al. 2011).

In order to obtain new insight into this scenario and the possible connection between  $\omega$  Cen and some of the low- $\alpha$  stars, our abundance analysis has been extended to include Mn, Cu, Zn, Y, and Ba. In the following Sect. 2, we describe how the abundances of these elements are determined and evaluate statistical and systematic errors. In Sect. 3, it is discussed if the metallicity trends and differences in abundance ratios between the two halo populations can be explained from current knowledge of the nucleosynthesis of elements in stars and supernovae. Furthermore, the abundance ratios of the low- $\alpha$  stars are compared with the

corresponding ratios in present-day Milky Way satellite galaxies and the  $\omega$  Cen globular cluster. Finally, some conclusions are given in Sect. 4.

## 2. Derivation of abundances

### 2.1. Methods

Elemental abundances are derived from a model-atmosphere analysis of equivalent widths (EWs) measured in high signal-to-noise (S/N), high-resolution spectra observed either with the ESO/VLT UVES spectrograph or the FIES spectrograph at the Nordic Optical Telescope (NOT). Details on wavelength range, resolution, and S/N are given in NS10. Figure 1 shows a comparison of the spectra of a high- and a low- $\alpha$  star in spectral bands containing some of the Mn, Cu, Zn, Y, and Ba lines applied in this paper.

As described in NS10, local thermodynamic equilibrium (LTE) is assumed and abundance ratios are determined relative to two bright thick-disk stars, HD 22879 and HD 76932. They are nearby stars for which  $T_{\text{eff}}$  can be determined from photometric colors, and  $\log g$  via Hipparcos parallaxes. Using a subset of the spectral lines for which the equivalent widths could be measured reliably in the solar flux spectrum (Kurucz et al. 1984), an abundance analysis relative to the Sun is carried out. Adopting these abundances, an ‘inverted’ analysis leads to the determination of  $gf$ -values for all lines. The derived  $gf$ -values for HD 22879 and HD 76932 agree within  $\pm 0.03$  dex for the large majority of lines; for each line, the mean value of  $gf$  is therefore adopted and used for the analysis of all program stars.

This procedure ensures a high internal precision of the abundance ratios. Relative to the Sun, the abundances are, however, more uncertain; line blending and continuum setting are often problematic in the solar spectrum, and non-LTE effects may be different for the Sun and a typical program star with  $[\text{Fe}/\text{H}] \sim -1$ . Thus, we find the average difference in Fe abundance derived from Fe II and Fe I lines to be  $[\text{Fe}/\text{H}]_{\text{II}} - [\text{Fe}/\text{H}]_{\text{I}} = 0.075$  dex for the two standard stars. This difference is probably caused by an over-ionization of Fe I with respect to LTE in the metal-poor stars (Asplund 2005).  $[\text{Fe}/\text{H}]_{\text{II}}$  is adopted as the metallicity parameter, but abundance ratios are based on lines from the same ionization stage, e.g.  $[\text{Mn}/\text{Fe}]$  is derived from Mn I and Fe I lines. Hence, if the non-LTE effects are the same for the two sets of lines,  $[\text{Mn}/\text{Fe}]$  is on the correct scale, but as discussed in Sect. 3.2.2 this may not be the case. Metallicity dependent departures from LTE could also affect the derived trends of abundance ratios as a function of  $[\text{Fe}/\text{H}]$ . However, when comparing stars with the same metallicity and within narrow ranges of  $T_{\text{eff}}$  and  $\log g$ , non-LTE effects are expected to be the same; the LTE approximation is therefore adequate in providing reliable differential abundances at a given metallicity.

For many program stars, colors are affected by interstellar reddening and the parallaxes are not accurate enough to determine reliable surface gravities. Thus,  $T_{\text{eff}}$  is determined from the excitation balance of weak ( $EW < 50 \text{ m}\text{\AA}$ ) Fe I lines, and  $\log g$  by requiring that the Fe abundances derived from Fe II and Fe I lines have the same difference as in the case of the standard stars, i.e. 0.075 dex.

Model atmospheres are interpolated from the new MARCS grid (Gustafsson et al. 2008), which includes two sets of models with different values of  $[\alpha/\text{Fe}]$ . Iteration is performed until the derived  $T_{\text{eff}}$ ,  $\log g$ ,  $[\text{Fe}/\text{H}]$ , and  $[\alpha/\text{Fe}]$  are consistent with the corresponding values of the model atmosphere.

<sup>1</sup>  $\alpha$  refers to the average abundance of Mg, Si, Ca, and Ti

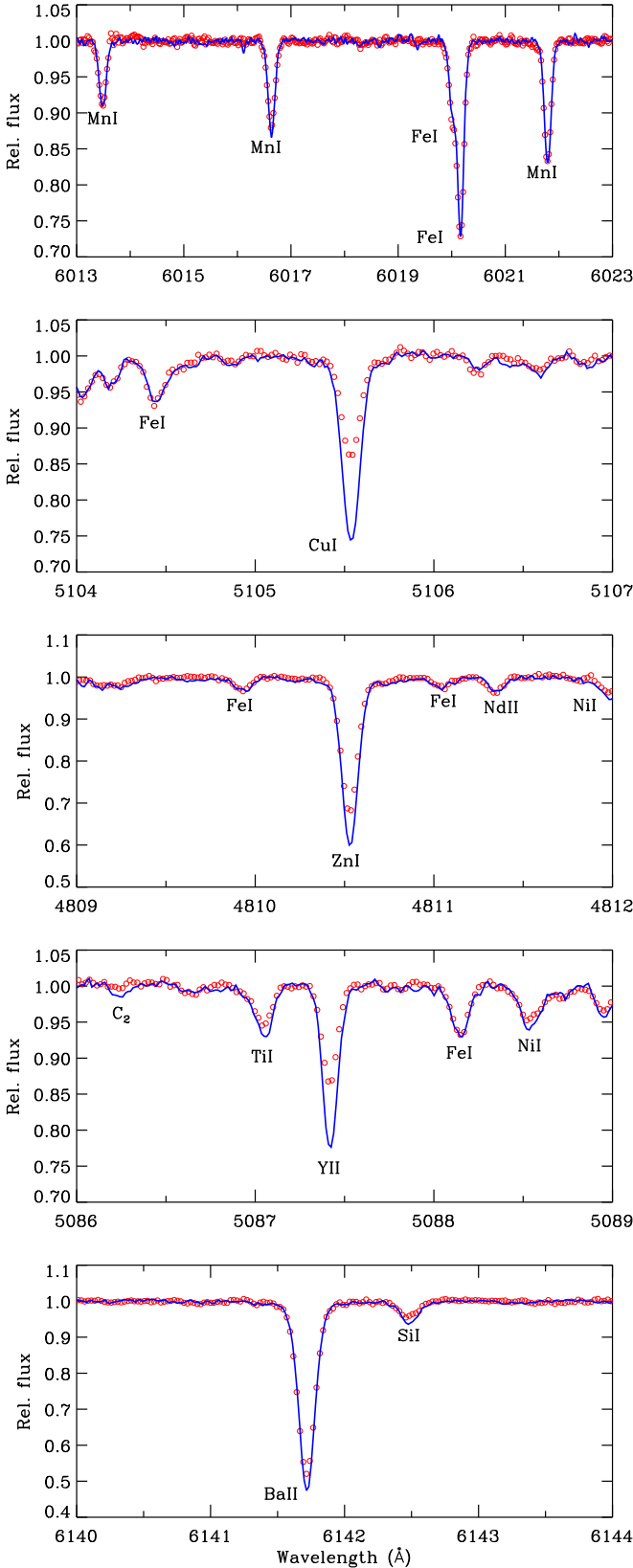


**Fig. 1.** Comparison of the spectra of a high- and a low- $\alpha$  star with similar atmospheric parameters and  $[\text{Fe}/\text{H}]$ . The spectrum of G 159-50 ( $T_{\text{eff}} = 5624 \text{ K}$ ,  $\log g = 4.37$ ,  $[\text{Fe}/\text{H}] = -0.93$ ,  $[\alpha/\text{Fe}] = 0.31$ ) is shown with a full drawn (blue) line, and that of CD -45 3283 ( $T_{\text{eff}} = 5597 \text{ K}$ ,  $\log g = 4.55$ ,  $[\text{Fe}/\text{H}] = -0.91$ ,  $[\alpha/\text{Fe}] = 0.12$ ) with open (red) circles. The strengths of the Mn and Fe lines are about the same in the two stars, whereas the Cu, Zn, Y, and Ba lines are weaker in the low- $\alpha$  star.

In the following, the determination of the abundances of Mn, Cu, Zn, Y, and Ba is described in some detail. Line broadenings caused by microturbulence and collisional damping are included. The microturbulence velocity is obtained by minimizing the dependence of  $[\text{Fe}/\text{H}]$  on the equivalent widths of Fe I lines with  $\chi_{\text{exc}} > 3.0 \text{ eV}$ . The cross sections for collisional broadening of Mn I, Cu I, Zn I, and Ba II lines are taken from Anstee & O'Mara (1995), Barklem & O'Mara (1997), and Barklem et al. (2000). For Y II lines, the Unsöld (1955) approximation to the Van der Waals interaction constant, enhanced by a factor of two, is adopted. The Y II lines employed are quite weak ( $EW \lesssim 60 \text{ mÅ}$ ), and are therefore not much affected by possible errors in the collisional cross sections.

Abundances of Zn, Y, and Ba are determined from equivalent widths using the Uppsala EQWIDTH code. For the Mn and Cu lines, which are significantly affected by hyperfine splitting (HFS), the BSYN code is applied to calculate equivalent widths as a function of abundance. Interpolation to the measured equivalent width then provides the stellar abundance value. Results based on UVES and FIES spectra are given in Tables 1 and 2, respectively, together with data for  $T_{\text{eff}}$ ,  $\log g$ ,  $[\text{Fe}/\text{H}]$ , and  $[\alpha/\text{Fe}]$  as determined in NS10. In addition, spectral line data and equivalent widths measured from UVES spectra of some selected stars (including the prototypes of a low- and a high- $\alpha$  star, CD -45 3283 and G 159-50) are given in Table 3. The complete Table 3 with equivalent widths for all UVES and FIES stars is available at the CDS.

## 2.2. Manganese

The derived abundances are based on Mn I lines at 4783.4, 4823.5, 6013.5, 6016.7, and 6021.8 Å with HFS data adopted from Prochaska et al. (2000). Cunha et al. (2010) used the same reference when deriving Mn abundances for giant stars in  $\omega \text{ Cen}$ , and tested that the more recent HFS data of Bergemann et al. (2007) changed the equivalent widths of the  $\lambda 6013.5$  line by less than 1 %.

The lines near 6000 Å are quite weak in our stellar spectra ( $EW \lesssim 50 \text{ mÅ}$ ) and disappear in the noise at low metallicities ( $[\text{Fe}/\text{H}] \lesssim -1.4$ ). The  $\lambda\lambda 4783.4, 4823.5$  lines are stronger, and are disregarded for the cooler and more metal-rich stars if their equivalent widths exceed 80 mÅ. Furthermore, the spectral coverage of the UVES spectra stops at 4780 Å, so in some cases the  $\lambda 4783.4$  line is lost because of a high negative radial velocity of the star.

For a group of 33 intermediate metallicity stars, all five Mn lines could be used to determine abundances, and it was checked that the Mn abundance derived from a given line is consistent with that derived from the other lines. The rms difference of Mn abundances derived from a single line and from all lines never exceeded 0.03 dex. This suggests that very precise Mn abundances have been obtained.

The derived  $[\text{Mn}/\text{Fe}]$  values are shown in Fig. 2 (upper panel)<sup>2</sup> as a function of  $[\text{Fe}/\text{H}]$  with different symbols employed for thick-disk, high- $\alpha$ , and low- $\alpha$  halo stars. The scatter in  $[\text{Mn}/\text{Fe}]$  at a given  $[\text{Fe}/\text{H}]$  is small ( $\approx 0.04 \text{ dex}$ ) and the metallicity trends for high- and low- $\alpha$  halo stars are nearly the same. The similarity of  $[\text{Mn}/\text{Fe}]$  for high- and low- $\alpha$  stars is also evident from Fig. 1, where the three Mn I lines near 6000 Å are

<sup>2</sup> For six stars observed with both UVES and FIES, only the UVES data are plotted in all figures. Table 4 shows a comparison between the two datasets.

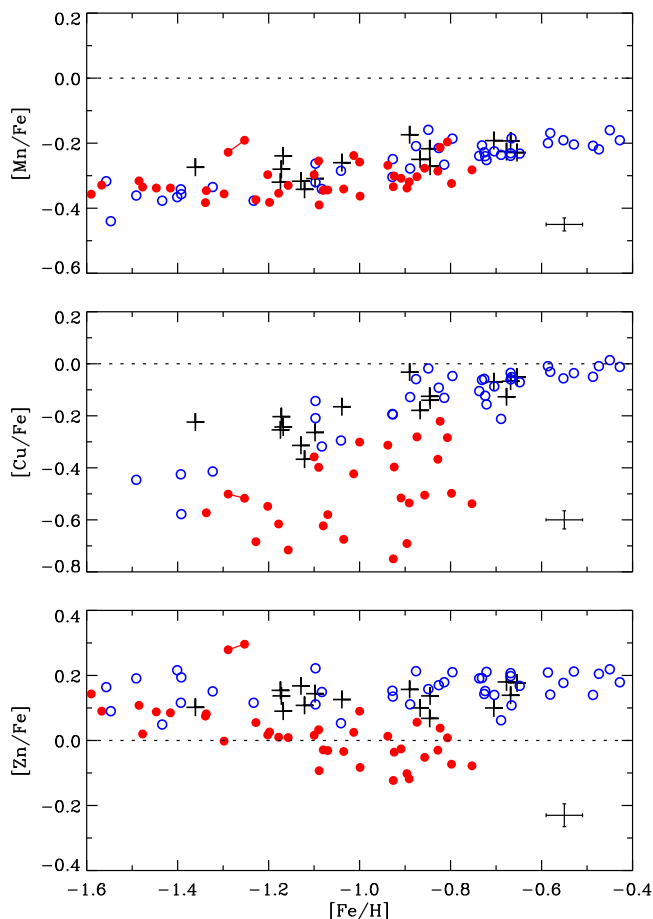


**Fig. 2.**  $[\text{Mn}/\text{Fe}]$ ,  $[\text{Cu}/\text{Fe}]$ , and  $[\text{Zn}/\text{Fe}]$  versus  $[\text{Fe}/\text{H}]$ . Stars belonging to the high- $\alpha$  halo population, as classified from  $[\text{Mg}/\text{Fe}]$ , are shown with open circles (blue in the online version), and the low- $\alpha$  halo population with filled (red) circles. The crosses refer to thick-disk stars. Typical one-sigma error bars are given in the lower, right corners. The two components of a binary star, G 112-43 and G 112-44, are connected by a straight line.

compared for two stars having nearly the same values of  $T_{\text{eff}}$ ,  $\log g$ , and  $[\text{Fe}/\text{H}]$ , but a significant difference in  $[\alpha/\text{Fe}]$ .

The only two stars, G 112-43 and G 112-44, deviating significantly from the average trend in Fig. 2, are probably components in a binary star. They are separated by only 11 arcsec on the sky and have nearly the same radial velocities and proper motions. G 112-43 is at the turn-off, and G 112-44 is a main-sequence star about one magnitude fainter. Both components belong to the class of low- $\alpha$  halo stars. In all abundance diagrams in the present paper and in NS10, these two stars are connected with a straight line. Their abundances agree very well, but they tend to deviate from the rest of the low- $\alpha$  stars in several abundance ratios. Interestingly, the two stars also stand out by having exceptionally high velocity components perpendicular to the Galactic plane (see Fig. 8 in NS10).

### 2.3. Copper

Cu abundances are derived from the equivalent widths of Cu I lines at 5105.5, 5218.2 and 5782.1 Å with HFS data taken from the same source as in the case of Mn (Prochaska et al. 2000).

Their data include isotopic splitting between  $^{63}\text{Cu}$  and  $^{65}\text{Cu}$  assuming solar system fractions of 0.69 and 0.31, respectively. The isotopic splitting is small and the calculated equivalent width is insensitive to the assumed isotopic composition.

The strongest of the three Cu lines,  $\lambda$  5105.5, is somewhat affected by blends of  $\text{C}_2$  molecular lines in the wings, and care was taken to avoid them by measuring equivalent widths using the deblending routine in the IRAF *splot* task. In general, the Cu lines become too faint ( $EW \lesssim 2 \text{ mÅ}$ ) to provide reliable abundances in the most metal-poor stars. Furthermore, the  $\lambda$  5782.1 line is not available in the UVES spectra, because it happens to fall in a gap between the two CCDs in the red arm of the spectrograph.

Cu abundances derived from the individual lines agree well. There is no significant systematic offsets, and a comparison of Cu abundances derived from the 5105.5 and 5218.2 Å lines results in a rms deviation of 0.052 dex. Cu abundances from the 5218.2 and 5782.1 Å lines in the FIES spectra have a rms deviation of 0.061 dex.

As seen from Fig. 2 (middle panel), the high- $\alpha$  and thick-disk stars define a smooth relation between  $[\text{Cu}/\text{Fe}]$  and  $[\text{Fe}/\text{H}]$ . The low- $\alpha$  stars, on the other hand, fall below the high- $\alpha$  stars and have a large scatter in  $[\text{Cu}/\text{Fe}]$  at a given metallicity. As an example of the difference in the strength of Cu lines for high- and low- $\alpha$  stars, Fig. 1 shows the  $\lambda$  5105.5 line in the spectra of G 159-50 and CD -45 3283.

### 2.4. Zinc

Abundances of Zn are determined from the Zn I  $\lambda\lambda$  4722.1, 4810.5 lines. The first line falls outside the range of the UVES spectra, but since these spectra have higher S/N than those obtained with FIES, it is estimated that the error of the Zn abundances is about the same for the two sets of observations. A comparison of abundances obtained from the two lines in the FIES spectra results in a rms deviation of 0.045 dex.

The relation between  $[\text{Zn}/\text{Fe}]$  and  $[\text{Fe}/\text{H}]$  is shown in Fig. 2 (lower panel). There is a clear difference in the trends of high- and low- $\alpha$  stars. The thick-disk and high- $\alpha$  halo stars have the same, near-constant  $[\text{Zn}/\text{Fe}] \approx 0.15$  with a rms scatter of 0.045 dex around this value. The low- $\alpha$  stars show a declining trend with increasing  $[\text{Fe}/\text{H}]$ , and are separated from the high- $\alpha$  stars in the metallicity range  $-1.4 < [\text{Fe}/\text{H}] < -0.7$ , except for the components of the binary star.

### 2.5. Yttrium

The yttrium abundances are based on the Y II lines at 4883.7 and 5087.4 Å. Being an odd-Z element ( $Z = 39$ ) HFS is present, but as discussed by Hannaford et al. (1982), the splitting of the hyperfine components is less than 1 mÅ and can be safely neglected in connection with the determination of Y abundances. The equivalent widths of the lines range from about 4 to 60 mÅ in our sample of stars, and the Y abundances derived from the two lines agree with a rms difference of 0.044 dex. From the outset, Y II lines at 5123.2 and 5200.4 Å were also included, but it turned out that the corresponding Y abundances deviate from the  $\lambda\lambda$  4883.7, 5087.4 abundances in a systematic way as a function of line strength indicating the presence of undetected blends.

Fig. 3 (upper panel) shows  $[\text{Y}/\text{Fe}]$  as a function of  $[\text{Fe}/\text{H}]$ . Although the low- $\alpha$  stars tend to have lower  $[\text{Y}/\text{Fe}]$  values than the high- $\alpha$  stars, there is considerable scatter in  $[\text{Y}/\text{Fe}]$ ; several of the thick-disk and high- $\alpha$  stars fall among the low-alpha

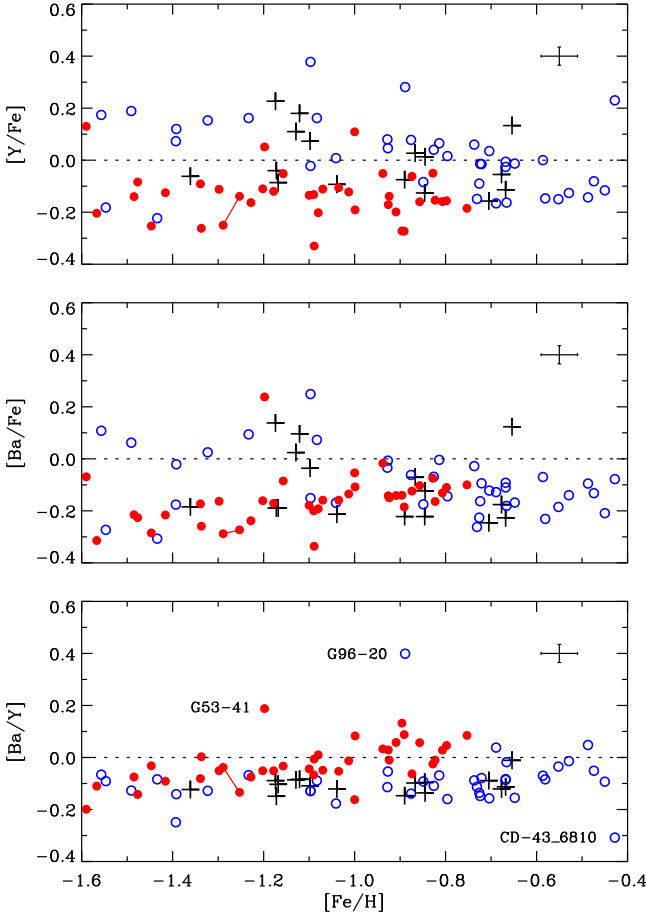


**Fig. 3.**  $[Y/Fe]$ ,  $[Ba/Fe]$ , and  $[Ba/Y]$  versus  $[Fe/H]$  with the same symbols as in Fig. 2.

stars. In addition, it should be noted that one star, G 24-25, has  $[Y/Fe] = 0.82$  and falls above the upper limit of the figure. This star is also very overabundant in Ba and other  $s$ -process elements with an abundance pattern that may be explained by mass transfer from an AGB companion (L. Shu et al., in preparation). According to Latham et al. (2002), G 24-25 is an SB1 spectroscopic binary with an orbital period of 9.45 years.

## 2.6. Barium

Abundances of Ba are determined from the  $\lambda\lambda 5853.7, 6141.7$  Ba II lines. Odd numbered Ba isotopes exhibit hyperfine splitting, and it was therefore first investigated if this has any significant effect on the derived abundances. Adopting HFS data from McWilliam (1998), profiles and equivalent widths were calculated for some representative stars. Contrary to the case of the Ba II line at  $4554.0\text{\AA}$  (e.g. Collet et al. 2009), the HFS effect on the  $\lambda\lambda 5853.7, 6141.7$  lines is small and changes the derived Ba abundances by less than 0.01 dex even if one assumes a pure  $r$ -process distribution of the isotopes instead of a solar system distribution. Thus, the abundance analysis was carried out neglecting hyperfine splitting.

The  $\lambda 5853.7$  Ba II line is suitable for precise abundance determination by having equivalent widths from about 10 to 60 mÅ in the majority of our stars. The  $\lambda 6141.7$  line has equivalent widths typically in the range 50 - 100 mÅ, and is therefore more

sensitive to the adopted microturbulence and damping constant. Nevertheless, the two sets of Ba abundances show a satisfactory agreement; the rms difference is 0.058 dex.

Fig. 3 (middle panel) shows  $[Ba/Fe]$  versus  $[Fe/H]$ . Like in the case of  $[Y/Fe]$ , there is some mixing of high- and low- $\alpha$  stars. The  $s$ -process rich star, G 24-25, has  $[Ba/Fe] = 1.45$  and falls far above the upper limit of the figure. The same is the case with G 96-20, a mildly  $s$ -process rich star, which has  $[Ba/Fe] = 0.68$  and  $[Y/Fe] = 0.28$ .

Interestingly, there is a correlation between the scatter in  $[Y/Fe]$  and  $[Ba/Fe]$  at a given metallicity. This is evident from the lower panel of Fig. 3, where  $[Ba/Y]$  is plotted vs.  $[Fe/H]$ . The high- and low- $\alpha$  stars show well-defined trends of  $[Ba/Y]$  with increasing separation as a function of increasing  $[Fe/H]$ . Still, a few stars deviate very significantly from these trends. G 24-25 with  $[Ba/Y] = 0.64$  falls above the limit of the figure, whereas the other  $s$ -process rich star, G 96-20, has  $[Ba/Y] = 0.40$ . Other deviating stars are G 53-41 (Na-rich according to NS10) and CD -43 6810.

## 2.7. Statistical errors

An estimate of the statistical errors of the various abundance ratios can be obtained by comparing values derived from UVES and FIES spectra for six stars observed with both instruments. As the atmospheric parameters are determined spectroscopically, the comparison will include the effect of the uncertainties in  $T_{\text{eff}}$ ,  $\log g$ , and  $[Fe/H]$  on the abundance ratios.

The results from this comparison are given in Table 4. The six stars are representative for the whole sample of program stars. G 20-15 is one of the most metal poor stars, HD 148816 and HD 179626 belong to the metal-rich end, and HD 189558, HD 193901 and HD 194598 have intermediate metallicities. As seen from the table, the systematic offsets between the UVES and FIES results are small and can be neglected. The rms scatters of the differences are on the same order of size as the errors of the average abundances estimated from comparing abundances derived from individual lines. Thus, the uncertainty of the atmospheric parameters is not adding much to the error budget, which can be ascribed to the fact that we are deriving abundance ratios from lines belonging to the same ionization stage.

On the basis of Table 4 and the line-to-line scatter of derived abundances, we estimate the one-sigma error of  $[Mn/Fe]$  to be 0.025 dex and the errors of other ratios to be 0.035 dex. It is emphasized that these are statistical errors that can be applied when comparing relative abundance ratios for stars at a given metallicity. The absolute values and the trends of abundance ratios as a function of metallicity may be affected by systematic errors caused by non-LTE effects as mentioned in Sect. 2.1.

## 3. Discussion

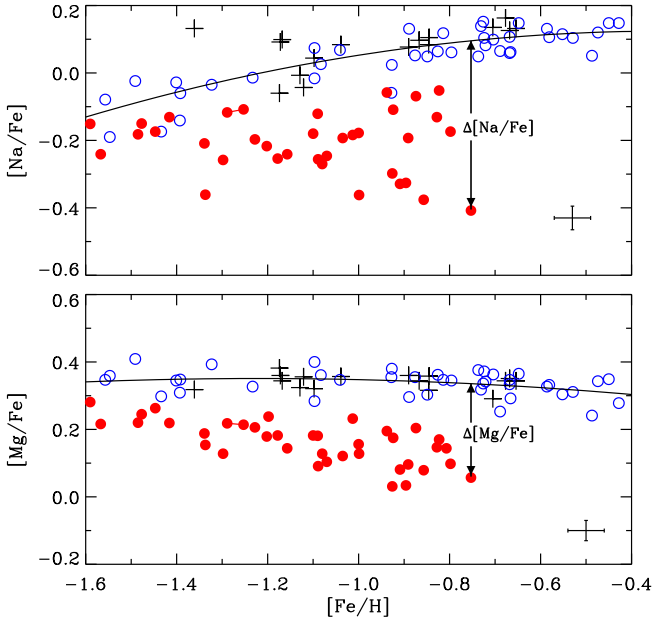
In this section, the trends and correlations in the elemental abundance ratios for high- and low- $\alpha$  halo stars are discussed in terms of nucleosynthesis calculations. Furthermore, the abundance ratios for the low-alpha stars are compared with ratios determined for dwarf galaxies and the  $\omega$  Cen globular cluster in an attempt to find evidence for a connection.

### 3.1. Differences and correlations between abundance ratios

As seen from Figs. 2 and 3, the high- and low- $\alpha$  halo stars begin to separate in  $[Cu/Fe]$ ,  $[Zn/Fe]$ , and  $[Ba/Y]$  at  $[Fe/H] \sim -1.5$

**Table 4.** Differences (UVES – FIES) of atmospheric parameters and abundance ratios determined from spectra of six stars observed with both instruments.

	$\Delta T_{\text{eff}}$ [K]	$\Delta \log g$	$\Delta[\text{Fe}/\text{H}]$	$\Delta[\text{Mn}/\text{Fe}]$	$\Delta[\text{Cu}/\text{Fe}]$	$\Delta[\text{Zn}/\text{Fe}]$	$\Delta[\text{Y}/\text{Fe}]$	$\Delta[\text{Ba}/\text{Fe}]$
G 20-15	-45	-0.04	-0.07	+0.011		+0.016	-0.046	-0.060
HD 148816	-17	-0.01	-0.03	-0.001	+0.021	+0.068	-0.011	+0.016
HD 179626	-5	-0.06	-0.04	+0.023	-0.062	-0.026	-0.046	-0.034
HD 189558	-6	-0.01	0.00	-0.025	-0.008	-0.018	+0.001	+0.014
HD 193901	-20	-0.05	-0.02	-0.001	-0.018	-0.033	+0.032	+0.044
HD 194598	+16	+0.01	-0.01	+0.020	-0.035	+0.020	+0.008	+0.003
Average( $\Delta$ )	-13	-0.03	-0.03	+0.005	-0.020	+0.004	-0.010	-0.003
rms( $\Delta$ )	23	0.04	0.04	0.017	0.034	0.035	0.030	0.035

**Fig. 4.** Definition of  $\Delta[\text{Na}/\text{Fe}]$  and  $\Delta[\text{Mg}/\text{Fe}]$ . The same symbols as in Fig. 2 are employed. The lines show quadratic fits to the distribution of thick-disk and high- $\alpha$  halo stars.

and reach the largest separation for the highest metallicities of the low- $\alpha$  stars. A similar behavior of  $[\text{Na}/\text{Fe}]$ ,  $[\text{Mg}/\text{Fe}]$ ,  $[\text{Si}/\text{Fe}]$ ,  $[\text{Ca}/\text{Fe}]$ ,  $[\text{Ti}/\text{Fe}]$ , and  $[\text{Ni}/\text{Fe}]$  is found in NS10. Furthermore, the low- $\alpha$  stars tend to have a larger scatter of these abundance ratios than the high- $\alpha$  stars.  $[\text{Cr}/\text{Fe}]$  and  $[\text{Mn}/\text{Fe}]$ , on the other hand, show little, if any, difference between the two halo populations, and the scatter in these ratios is about the same for the two groups.

In order to quantify the differences between the two halo populations, we have made quadratic fits to the trends of abundance ratios as a function of  $[\text{Fe}/\text{H}]$  for the thick-disk and high- $\alpha$  halo stars. As an example, Fig. 4 shows the fits to  $[\text{Na}/\text{Fe}]$  and  $[\text{Mg}/\text{Fe}]$ . For a given star, the deviations from the fits,  $\Delta[\text{Na}/\text{Fe}]$  and  $\Delta[\text{Mg}/\text{Fe}]$ , are defined as shown on the figure. Corresponding quadratic fits and deviations are calculated for the other element ratios. Table 5 gives the mean value and the rms scatter of the deviations for the metallicity range  $-1.1 \leq [\text{Fe}/\text{H}] < -0.7$ , where the largest separation of the two populations occurs. The high- $\alpha$  group includes 18 halo stars and 7 thick-disk stars, and the low- $\alpha$  group comprises 21 halo stars, except in the case of copper, for which two stars have too weak Cu I lines to allow a reliable determination of the Cu abundance.

**Table 5.** Mean value and rms scatter of deviations in abundance ratios for high- and low- $\alpha$  stars with  $-1.1 \leq [\text{Fe}/\text{H}] < -0.7$ .

[X1/X2]	High- $\alpha$ group		Low- $\alpha$ group	
	$\langle \Delta[\frac{X1}{X2}] \rangle$	$\sigma(\Delta[\frac{X1}{X2}])$	$\langle \Delta[\frac{X1}{X2}] \rangle$	$\sigma(\Delta[\frac{X1}{X2}])$
[Na/Fe]	0.000	0.041	-0.277	0.110
[Mg/Fe]	0.002	0.029	-0.217	0.055
[Si/Fe]	0.001	0.028	-0.175	0.040
[Ca/Fe]	0.002	0.030	-0.072	0.046
[Ti/Fe]	0.003	0.030	-0.137	0.056
[Cr/Fe]	0.004	0.032	-0.031	0.029
[Mn/Fe]	0.003	0.036	-0.043	0.042
[Ni/Fe]	0.001	0.012	-0.127	0.035
[Cu/Fe]	0.006	0.056	-0.307	0.152
[Zn/Fe]	0.002	0.042	-0.172	0.061
[Y/Ba]	0.002	0.031	-0.123	0.066

As seen from Table 5, the mean value of the deviations is close to zero for the group of high- $\alpha$  stars, as one would expect from the definition of  $\Delta$ , and the scatter is not much higher than expected from the estimated error of the abundance ratios. For the group of low- $\alpha$  stars the mean value of  $\Delta$  is always negative and the scatter is significantly higher than the scatter for the high- $\alpha$  group except in the case of Cr and Mn.

As shown in Fig. 5, there are remarkable correlations between the deviations in the various abundance ratios. Choosing  $\Delta[\text{Na}/\text{Fe}]$  as the abscissa, one sees very significant correlations for  $[\text{Mg}/\text{Fe}]$ ,  $[\text{Si}/\text{Fe}]$ ,  $[\text{Ti}/\text{Fe}]$ ,  $[\text{Ni}/\text{Fe}]$ ,  $[\text{Cu}/\text{Fe}]$ ,  $[\text{Zn}/\text{Fe}]$ , and  $[\text{Y}/\text{Ba}]$ . The correlation is less clear in the case of  $[\text{Ca}/\text{Fe}]$ , and the distributions of  $\Delta[\text{Cr}/\text{Fe}]$  and  $\Delta[\text{Mn}/\text{Fe}]$  are nearly flat.

One may ask if the abundance differences between high- and low- $\alpha$  stars, and the correlations seen in Fig. 5 could be spurious, due to errors in  $T_{\text{eff}}$  and/or  $\log g$ . This is, however, not the case. As shown in Fig. 6,  $\Delta[\text{Mg}/\text{Fe}]$  has no significant dependence on  $T_{\text{eff}}$  or  $\log g$  and the same is the case for the other abundance ratios. Furthermore, the distribution of stars as a function of  $T_{\text{eff}}$  and  $\log g$  is similar for the high- and low- $\alpha$  populations, except for one interesting detail; the maximum  $T_{\text{eff}}$  for the low- $\alpha$  stars is approximately 150 K higher than the maximum for the high- $\alpha$  group. These maxima are likely to correspond to the turnoff-points in the HR-diagram for the two populations, and depend on the ages of the stellar populations as well as  $[\text{Fe}/\text{H}]$  and  $[\alpha/\text{Fe}]$ . Using the position of stars in the  $\log g - T_{\text{eff}}$  diagram to derive individual ages, Schuster et al. (in preparation) find that in fact stars in the low- $\alpha$  population are on the average 2-3 Gyr younger than stars belonging to the high- $\alpha$  population.

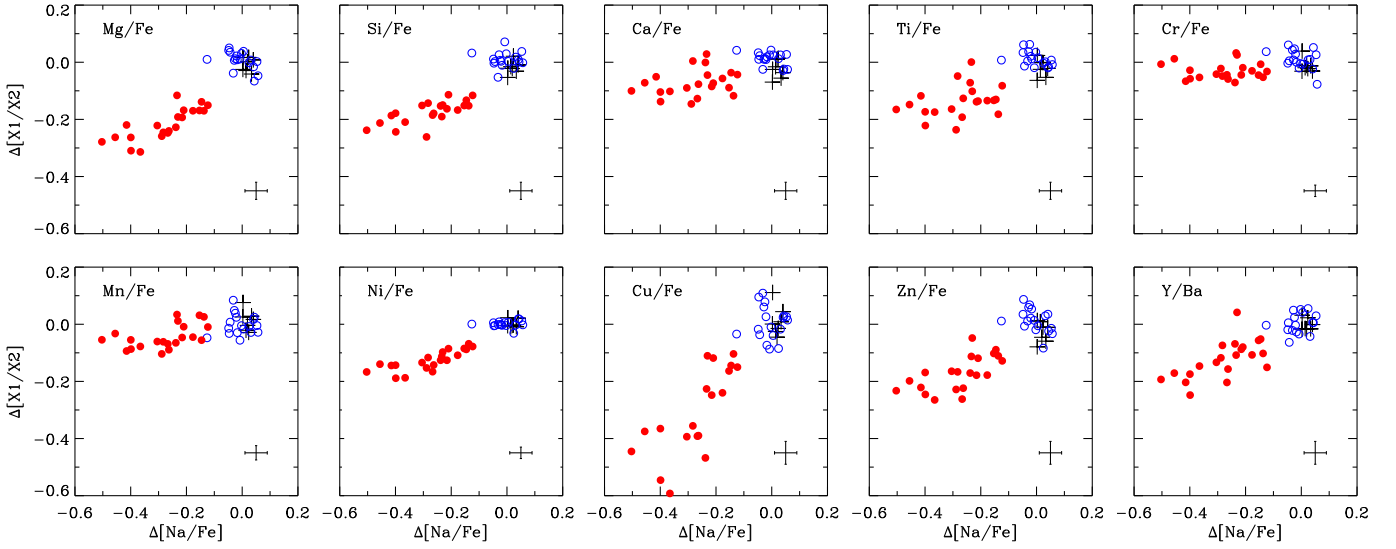


**Fig. 5.** Correlation between differences in abundance ratios relative to quadratic fits to the metallicity trends for thick-disk and high- $\alpha$  halo stars (see Fig. 4). Only stars in the metallicity range  $-1.1 \leq [\text{Fe}/\text{H}] < -0.7$  are plotted. The same symbols as in Fig. 2 are employed.

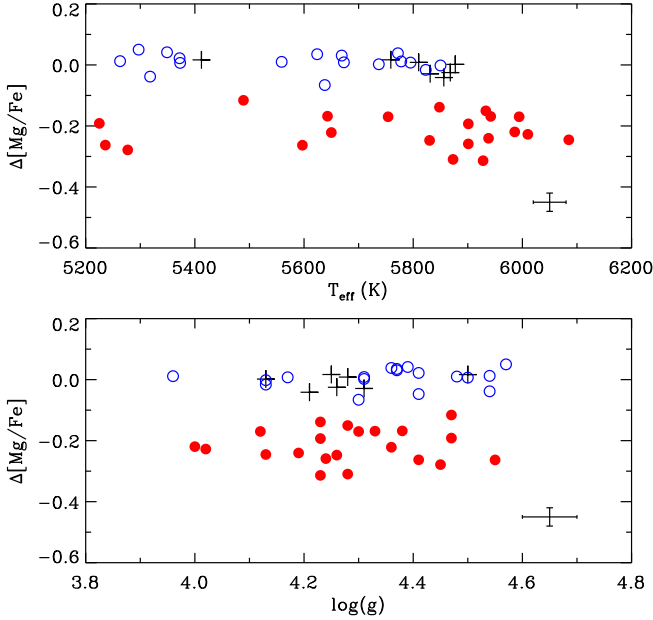


**Fig. 6.**  $\Delta[\text{Mg}/\text{Fe}]$  vs.  $T_{\text{eff}}$  and  $\log g$  for stars in the metallicity range  $-1.1 \leq [\text{Fe}/\text{H}] < -0.7$ . The same symbols as in Fig. 2 are employed.

### 3.2. Comparison with nucleosynthesis calculations

#### 3.2.1. The $\alpha$ -capture elements and sodium

Magnesium is a product of hydrostatic carbon and neon burning in massive stars and is dispersed to the interstellar medium by SNe II (e.g. Woosley & Weaver 1995). Very little Mg is produced by SNe Ia (Nomoto et al. 1997). Our comparison element, iron, partly comes from explosive oxygen and silicon burning in SNe II, but is also produced by SNe Ia; according to Tsujimoto et al. (1995) about 60% of iron in the Sun originates from these less massive supernovae. The downward trend of  $[\text{Mg}/\text{Fe}]$  with increasing metallicity for the low- $\alpha$  population may therefore

be explained by delayed contribution of iron from SNe Ia, as first suggested by Tinsley (1979) in a discussion of the trend of  $[\text{O}/\text{Fe}]$  vs.  $[\text{Fe}/\text{H}]$  for Galactic halo and disk stars.

The near-constancy of  $[\text{Mg}/\text{Fe}]$  for the high- $\alpha$  population indicates that these stars have been formed in regions with a relatively high SFR, such that only SNe II have contributed to the chemical evolution up to  $[\text{Fe}/\text{H}] \sim -0.4$ . The low- $\alpha$  stars, on the other hand, originate from systems with a slower chemical evolution, where SNe Ia have started to contribute iron at a metallicity  $[\text{Fe}/\text{H}] \lesssim -1.5$ . Good candidates for such systems are dwarf galaxies, for which the chemical evolution is thought to proceed slowly because of a low SFR and/or loss of produced elements in galactic winds (e.g. Lanfranchi & Matteucci 2003; Fenner et al. 2006).

Sodium is produced by hydrostatic carbon burning in massive stars with a yield that depends on the neutron excess (e.g. Kobayashi et al. 2006). Neutrons are released by the  $^{22}\text{Ne}(\alpha, n)^{25}\text{Mg}$  reaction, where  $^{22}\text{Ne}$  comes from double  $\alpha$ -capture on  $^{14}\text{N}$ , which is enhanced in the CNO cycle during hydrogen burning at the expense of carbon and oxygen. As a result, the efficiency of Na production increases with the original C and O abundances of the star. This explains the rising trend of  $[\text{Na}/\text{Fe}]$  vs.  $[\text{Fe}/\text{H}]$  for the high- $\alpha$  stars in Fig. 4. SNe Ia do not make Na in any significant amount (Nomoto et al. 1997), so the underabundance of Na relative to Fe in low- $\alpha$  stars, and the correlation between  $\Delta[\text{Na}/\text{Fe}]$  and  $\Delta[\text{Mg}/\text{Fe}]$  (Fig. 5) is partly due to the excess of iron produced by SNe Ia. The amplitude of the variations in  $[\text{Na}/\text{Fe}]$  is, however, significantly larger than in the case of  $[\text{Mg}/\text{Fe}]$  (Table 5). We suggest that this is connected to the CO dependent yield of Na; at a given  $[\text{Fe}/\text{H}]$ , the low- $\alpha$  massive stars synthesizing Na contain less carbon and oxygen than massive stars belonging to the high- $\alpha$  population<sup>3</sup>.

In addition to Na production in massive stars, sodium may also be made in hydrogen burning shells of intermediate mass AGB stars in connection with the CNO and Ne-Na cycles

<sup>3</sup> We have not yet made a quantitative analysis of the abundances of C and O, but a comparison of spectra for stars with similar  $T_{\text{eff}}$ ,  $\log g$ , and  $[\text{Fe}/\text{H}]$  shows that low- $\alpha$  stars have weaker C I and O I lines than high- $\alpha$  stars.

(Ventura et al. 2001). This process is often assumed to be responsible for the high Na abundances and the Na–O anti-correlation in globular cluster stars (Carretta et al. 2009). If this process had contributed significantly to the chemical evolution of the low- $\alpha$  population, one would not expect such a clear correlation between  $[\text{Na}/\text{Fe}]$  and  $[\text{Mg}/\text{Fe}]$  as seen in Fig. 5. As mentioned in NS10, there are, however, two Na-rich stars among the low- $\alpha$  population (G 53-41 with  $[\text{Na}/\text{Fe}] = 0.23$  and G 150-40 with  $[\text{Na}/\text{Fe}] = 0.28$ ) falling outside the boundaries of Figs. 4 and 5. These stars could be halo field counterparts of the Na-enhanced globular cluster stars, formed in the vicinity of an intermediate mass AGB star before its nucleosynthesis products were mixed into the interstellar medium.

The remaining  $\alpha$ -capture elements, Si, Ca, and Ti are made by oxygen and silicon burning in massive stars, but also have a significant contribution from SNe Ia. According to Tsujimoto et al. (1995, Table 3), the relative contributions of SNe Ia to the solar abundances are negligible for Mg, 17% for Si, 25% for Ca, and 57% for Fe. This explains why the amplitudes of the variations in  $[\text{Si}/\text{Fe}]$  and  $[\text{Ca}/\text{Fe}]$  are smaller than in the case of  $[\text{Mg}/\text{Fe}]$  (Table 5). It is, however, puzzling that the variation in  $[\text{Ca}/\text{Fe}]$  is so small compared to the variation in  $[\text{Mg}/\text{Fe}]$  (only about one-third). Titanium was not included in the calculations of Tsujimoto et al. (SNe II models underproduce Ti by a factor  $\gtrsim 2$ , e.g. Kobayashi et al. 2006), but according to Table 5 and Fig. 5, the amplitude of the  $[\text{Ti}/\text{Fe}]$  variations is larger than that of  $[\text{Ca}/\text{Fe}]$ .

### 3.2.2. Chromium and manganese

Chromium is produced by both Type II and Ia SNe. As seen from Fig. 6 in NS10,  $[\text{Cr}/\text{Fe}]$  is close to zero and there is no significant difference in  $[\text{Cr}/\text{Fe}]$  between high- and low- $\alpha$  stars. Thus, chromium follows iron closely. This agrees with the calculations of Kobayashi et al. 2006, who include nucleosynthesis contributions from both normal SNe II with explosion energy  $\sim 10^{51}$  erg, and more energetic core collapse SNe, so-called hypernovae (HNe) with 10 times higher explosion energy. For masses above  $20 M_{\odot}$ , the fraction of HNe is assumed to be 0.5. In addition, contribution from SNe Ia is taken into account with yields from Nomoto et al. (1997). The calculated  $[\text{Cr}/\text{Fe}]$  is close to zero for metallicities ranging from  $[\text{Fe}/\text{H}] \approx -3$  to solar.

Like in the case of  $[\text{Cr}/\text{Fe}]$ , there is no significant difference in  $[\text{Mn}/\text{Fe}]$  between high- and low- $\alpha$  stars, but  $[\text{Mn}/\text{Fe}]$  increases from about  $-0.4$  dex at  $[\text{Fe}/\text{H}] = -1.6$  to  $-0.2$  dex at  $[\text{Fe}/\text{H}] = -0.4$ . This trend continues for disk stars so that  $[\text{Mn}/\text{Fe}] \approx 0$  at solar metallicity (e.g. Feltzing et al. 2007).

Gratton (1989) suggested that the rise in  $[\text{Mn}/\text{Fe}]$  is caused by an overproduction of Mn relative to Fe in SNe Ia as also predicted from the yields of Nomoto et al. (1997). Accordingly, one would expect the low- $\alpha$  halo stars to lie above the  $[\text{Mn}/\text{Fe}]$  trend defined by the high- $\alpha$  stars, but this is not the case as seen from Fig. 2. The explanation may be that the Mn yields of SNe Ia are metallicity dependent as suggested from models by Badenes et al. (2008). They find that the increase in neutron excess with metallicity leads to a faster increase of Mn/Cr in Type Ia SNe than in core collapse SNe. Recalling that the SNe Ia which enrich the low- $\alpha$  population are relatively metal-poor, this may cancel the expected overabundance of  $[\text{Mn}/\text{Fe}]$  for the low- $\alpha$  population. In extreme systems such as the Sagittarius dwarf spheroidal (dSph) galaxy, the metallicity dependent Mn yield of SNe Ia may even lead to a decrease of  $[\text{Mn}/\text{Fe}]$  relative to the trend for disk stars as first suggested by McWilliam et al. (2003) and later

shown in detail by Cescutti et al. (2008) on the basis of chemical evolution models.

Kobayashi & Nomoto (2009) have argued that if the iron abundance of the progenitors of Type Ia SNe is lower than  $[\text{Fe}/\text{H}] \sim -1$ , then the wind of the white dwarf in a binary system is too weak for an explosion to occur. The absence of SNe Ia below  $[\text{Fe}/\text{H}] \sim -1$  could explain that the trend of  $[\text{Mn}/\text{Fe}]$  is the same for high- and low- $\alpha$  stars, but then one has to assume different initial mass functions (IMFs) for the two populations in order to explain the differences in  $[\alpha/\text{Fe}]$ . According to Kobayashi et al. (2006), an IMF biased towards low-mass SNe II would lead to lower values of  $[\alpha/\text{Fe}]$ , but because the difference in  $[\alpha/\text{Fe}]$  between the high- and low- $\alpha$  populations increases with  $[\text{Fe}/\text{H}]$ , one has to assume a very complicated behavior of the IMF, i.e. a metallicity dependent IMF for the low- $\alpha$  stars and a constant IMF for the high- $\alpha$  stars.

The rise in  $[\text{Mn}/\text{Fe}]$  with  $[\text{Fe}/\text{H}]$  for the high- $\alpha$  population cannot be explained as caused by SNe Ia, because the constancy of  $[\text{Mg}/\text{Fe}]$  excludes any significant contribution from SNe Ia. Instead, the rise could be due to a metallicity-dependent yield of Mn in SNe II, but the calculated yield ratio Mn/Fe show only a relatively weak increase with metallicity starting at  $[\text{Fe}/\text{H}] \sim -1.2$  (Kobayashi et al. 2006, Fig. 5). Perhaps our assumption of LTE is leading to a spurious increase in  $[\text{Mn}/\text{Fe}]$  with  $[\text{Fe}/\text{H}]$ . According to Bergemann & Gehren (2008), the strengths of Mn I lines are affected by departures from LTE; the non-LTE corrections on the derived Mn abundances are positive and increase with decreasing metallicity. When taken this into account, the trend of  $[\text{Mn}/\text{Fe}]$  becomes more flat and approaches  $[\text{Mn}/\text{Fe}] \sim 0$  at all metallicities.

### 3.2.3. Nickel and copper

It was long thought that nickel closely follows iron (i.e.  $[\text{Ni}/\text{Fe}] \approx 0$ ) in both halo and disk stars. Nissen & Schuster (1997) found, however,  $[\text{Ni}/\text{Fe}]$  to be slightly negative in eight halo stars having unusually low values of  $[\alpha/\text{Fe}]$  and  $[\text{Na}/\text{Fe}]$ . Even more negative values of  $[\text{Ni}/\text{Fe}]$  have been found in dSph galaxies (Venn et al. 2004). The underabundance of  $[\text{Ni}/\text{Fe}]$  for low- $\alpha$  stars is confirmed in NS10, and as seen from Fig. 5, there is a very tight correlation between  $\Delta[\text{Ni}/\text{Fe}]$  and  $\Delta[\text{Na}/\text{Fe}]$  for stars in the range  $-1.1 \leq [\text{Fe}/\text{H}] < -0.7$ .

As discussed in Venn et al. (2004), the correlation between Na and Ni, can be explained if the production of  $^{58}\text{Ni}$  (the most abundant Ni isotope) in SNe II depends on the neutron excess in the same way as  $^{23}\text{Na}$ , i.e. the yields of both elements are metallicity dependent. Ni is, however, also produced by SNe Ia. Current models of SNe Ia (e.g. Nomoto et al. 1997) predict an overproduction of Ni relative to Fe, and it is therefore puzzling that the low- $\alpha$  stars fall below the high- $\alpha$  group in the  $[\text{Ni}/\text{Fe}] - [\text{Fe}/\text{H}]$  diagram. Evidently, there is something wrong with the yield calculations. As noted by Kobayashi et al. (2006), the Ni yield from SNe Ia depends strongly on the electron excess,  $Y_e$ , in the burning region, which is sensitive to uncertain parameters such as the propagation speed of the burning front and the central density of the white dwarf progenitor. Hence, there seems to be room for a downward revision of Ni yields for SNe Ia.

The increase in  $[\text{Cu}/\text{Fe}]$  with  $[\text{Fe}/\text{H}]$  (Fig. 2) for the high- $\alpha$  stars, can be explained if copper is mainly produced in massive stars by the weak  $s$ -process (e.g. Bisterzo et al. 2004). The necessary neutrons come from the  $^{22}\text{Ne}(\alpha, n)^{25}\text{Mg}$  reaction, which also controls the production of Na. Thus, the efficiency of Cu production by the weak  $s$ -process also increases with increasing original CNO abundance. This is confirmed by detailed cal-

culations of yields by Kobayashi et al. (2006), who find a steep increase in Cu/Fe as a function of heavy element abundance.

Current SNe Ia models predict negligible Cu yields (e.g. Nomoto et al. 1997). The reduced Cu/Fe ratio in low- $\alpha$  stars therefore arises because they were formed from gas enriched with Fe from SNe Ia and with Cu produced by CNO-poor massive stars. The same type of explanation was suggested in Sect. 3.2.1 for the underabundance of [Na/Fe] in the low- $\alpha$  population. As seen from Fig. 5, there is indeed a nice correlation between  $\Delta[\text{Cu/Fe}]$  and  $\Delta[\text{Na/Fe}]$  with a slope that is close to one.

### 3.2.4. Zinc

The distribution of stars in the [Zn/Fe] - [Fe/H] diagram (Fig. 2) suggests that zinc behaves in much the same way as an  $\alpha$ -element. [Zn/Fe] is near-constant at a level of +0.15 dex for the thick-disk and high- $\alpha$  halo stars, whereas the low- $\alpha$  stars show a declining trend in [Zn/Fe] as a function of increasing [Fe/H] with an amplitude similar to that of [Si/Fe] (Table 5).

The heavy isotopes,  $^{66-70}\text{Zn}$ , are probably made by the weak  $s$ -process in massive stars (Bisterzo et al. 2004). According to Kobayashi et al. (2006), the most abundant isotope,  $^{64}\text{Zn}$ , is mainly formed by Si-burning in hypernovae. Type Ia SNe produce relatively little Zn. Hence, the decreasing trend of [Zn/Fe] in the low- $\alpha$  population may be explained by the production of iron in SNe Ia.

One may ask if the derived overabundance of Zn relative to Fe could be a spurious result because of the assumption of LTE. According to the statistical equilibrium calculations for the energy level populations of the Zn I atom by Takeda et al. (2005), the non-LTE corrections of Zn abundances derived from the  $\lambda\lambda 4722.1, 4810.5$  lines increase with decreasing metallicity and reach about +0.1 dex relative to the Sun for a main-sequence star with  $T_{\text{eff}} \simeq 5800$  K and [Fe/H]  $\simeq -1$ . This is of the same order of size as the non-LTE correction for the Fe abundance derived from Fe I lines (as estimated from the difference in Fe abundances derived from Fe II and Fe I lines; see Sect. 2.1). There is some uncertainty in the statistical calculations due to a poor knowledge of the cross section for collisions between Zn and H atoms, but altogether it is unlikely that the inclusion of non-LTE corrections would lead to systematic changes in the derived [Zn/Fe] values by more than  $\pm 0.1$  dex, and the difference in [Zn/Fe] between the high- and low- $\alpha$  stars at a given metallicity would not be affected.

When studying elemental abundances in the interstellar gas of damped Lyman-alpha systems (DLAs), it is often assumed that Zn can be used as a proxy for Fe. In support of this assumption, reference is given to the study of Zn abundances in halo and disk stars by Sneden et al. (1991). Zinc has the advantage of being a volatile element like sulfur, and is therefore not depleted onto interstellar grains. Thus, it has been suggested that the S/Zn ratio can be used to date the star formation process in DLAs in the same way as  $\alpha/\text{Fe}$  for stars. According to the present work Zn is, however, not a good proxy for Fe. Supporting evidence comes from the work of Bensby et al. (2005), who found an offset in [Zn/Fe] between thick- and thin-disk stars amounting to about 0.15 dex. Altogether, this means that S/Zn is not a sensitive tracer of the star formation history in galaxies. The same conclusion was reached by Nissen et al. (2007) from a direct study of [S/Zn] as a function [Fe/H] in Galactic stars.

### 3.2.5. Yttrium and barium

Yttrium and barium can be made by neutron capture onto iron-peak nuclei by the weak  $s$ -process in massive stars (like copper, see Sect. 3.2.3) as well as the  $r$ -process, which is also thought to take place in massive stars. From a Galactic evolution model, Travaglio et al. (2004) predict that both [Y/Fe] and [Ba/Fe] are close to zero in halo and thick-disk stars with [Fe/H]  $> -2$ . This is in rough agreement with the observed trend for high- $\alpha$  stars (Fig. 3), although there is a puzzlingly large scatter suggesting a poor degree of mixing of Y and Ba with Fe in the interstellar gas.

In addition, Y and Ba can be made by the main  $s$ -process occurring during shell He-burning in low-mass ( $M \lesssim 4 M_{\odot}$ ) AGB stars (Busso et al. 1999). Yttrium ( $Z = 39$ ) belongs to the group of light  $s$ -process ( $ls$ ) elements, whereas Ba ( $Z = 56$ ) is one of the heavy  $s$ -process ( $hs$ ) elements. The neutrons mainly come from the  $^{13}\text{C}(\alpha, n)^{16}\text{O}$  reaction, where  $^{13}\text{C}$  is made by proton capture onto  $^{12}\text{C}$  nuclei produced during He-burning. Hence, the neutron flux per seed (iron) nuclei increases with decreasing metallicity. This means that low-metallicity AGB stars produce a higher  $hs/ls$  ratio than high-metallicity AGB stars (Travaglio et al. 2004). The increasing trend of [Ba/Y] for the low- $\alpha$  stars (Fig. 3) may therefore be explained as due to delayed production of  $s$ -process elements by metal-deficient, low-mass AGB stars.

Given that the progenitors of low-mass AGB stars evolve on a timescale ranging from  $\sim 2 \times 10^8$  years to several billion years (Schaller et al. 1992), the [Ba/Y] trends in Fig. 3 support the idea that the low- $\alpha$  stars have been formed in systems with a slower chemical evolution than the regions from which the high- $\alpha$  and thick-disk stars originated. Detailed models for the chemical evolution of dSph galaxies including mass-loss in SNe winds (Fenner et al. 2006) confirm that an increase in Ba/Y for the metallicity range  $-2 < [\text{Fe/H}] < -1$  is obtained, when the star formation history extends over more than one Gyr.

### 3.3. Comparison with dSph and Irr galaxies

As discussed in NS10, the kinematics of the low- $\alpha$  stars suggest that they have been accreted from Milky-Way satellite galaxies. It is therefore interesting to compare abundance ratios measured in such present-day galaxies with the corresponding ratios for the low- $\alpha$  stars.

As reviewed by Tolstoy et al. (2009), the knowledge about elemental abundances in dwarf galaxies has been greatly improved over the last few years thanks to the advent of multi-object, high-resolution spectrographs at large telescopes allowing the determination of abundances for samples of red giant branch (RGB) stars. As seen from Fig. 11 in Tolstoy et al. (2009), dSph stars with low metallicities, [Fe/H]  $\lesssim -2$ , have about the same  $\alpha/\text{Fe}$  ratio as stars in the Galactic halo ([ $\alpha/\text{Fe}$ ]  $\sim +0.3$ ), which points to a common IMF. At some metallicity (the so-called ‘knee’ position, [Fe/H]<sub>knee</sub>), [ $\alpha/\text{Fe}$ ] starts to decrease as a function of increasing metallicity. This is similar to the trend for the low- $\alpha$  field stars except that the amplitude of the [ $\alpha/\text{Fe}$ ] variations tends to be larger for dSph galaxies than in the case of the low- $\alpha$  population in the solar neighborhood.

There is some evidence that [Fe/H]<sub>knee</sub> differs among the dwarf spheroidals and is correlated with the maximum [Fe/H] reached, i.e. that metallicity at which the gas is blown out of the system by SNe. The low-luminosity dSph systems, Carina, Draco, and Ursa Minor, have [Fe/H]<sub>knee</sub>  $\sim -2.4$  to  $-2.0$ , and [Fe/H]<sub>max</sub>  $\sim -1.5$  (Koch et al. 2008; Cohen & Huang 2009, 2010). The more luminous Sculptor dSph has [Fe/H]<sub>knee</sub>  $\sim -1.8$ ,

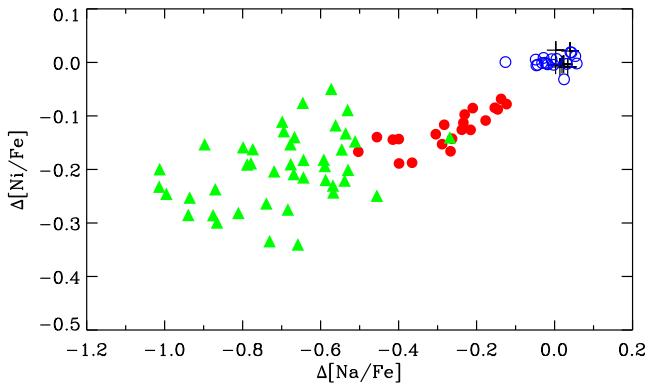


**Fig. 7.**  $\Delta[\text{Ni}/\text{Fe}]$  vs.  $\Delta[\text{Na}/\text{Fe}]$  for stars in the metallicity range  $-1.1 \leq [\text{Fe}/\text{H}] < -0.7$ . Stars in this paper are shown with the same symbols as in Fig. 2. Green triangles show values for RGB stars in the Fornax dSph galaxy (Letarte et al. 2010).

and  $[\text{Fe}/\text{H}]_{\text{max}} \sim -1.0$  (Tolstoy et al. 2009). In the case of the still more luminous Fornax system, the ‘knee’ position is not well defined, but  $[\text{Fe}/\text{H}]_{\text{max}} \sim -0.6$  (Letarte et al. 2010). Finally, the Sagittarius dSph has  $[\text{Fe}/\text{H}]_{\text{knee}} \sim -1.3$ , and  $[\text{Fe}/\text{H}]_{\text{max}} \sim 0.0$  (Sbordone et al. 2007; Carretta et al. 2010). This maximum metallicity occurs in the core of Sagittarius; the metallicity of stars in the trailing and leading arms (i.e. stars presently being accreted by the Galaxy) tend to be lower (Chou et al. 2007; Keller et al. 2010).

The ‘knee’ position for the low- $\alpha$  population is somewhat uncertain because no stars with  $[\text{Fe}/\text{H}] < -1.6$  were included. According to Fig. 1 in NS10, it seems to lie around or slightly below a metallicity of  $-1.5$ , i.e.  $[\text{Fe}/\text{H}]_{\text{knee}} \lesssim -1.5$ . The maximum metallicity for the low- $\alpha$  stars, on the other hand, is well-defined at  $[\text{Fe}/\text{H}]_{\text{max}} \simeq -0.75$ . Hence, there is no exact correspondence with any of the existing dSph systems, but this does not exclude that the low- $\alpha$  stars originate from now dissolved dSph systems. The reason for the scatter of  $[\alpha/\text{Fe}]$  at a given metallicity in the low- $\alpha$  population could be that they were accreted from an ensemble of dwarf galaxies with somewhat different star formation efficiencies.

For a more detailed comparison of abundance ratios in dSph galaxies and the low- $\alpha$  field stars, we may use Fornax as a well studied example (Letarte et al. 2010).  $[\text{Mg}/\text{Fe}]$  and  $[\text{Si}/\text{Fe}]$  overlap with the corresponding ratios for the low- $\alpha$  stars, but  $[\text{Ca}/\text{Fe}]$  and  $[\text{Ti}/\text{Fe}]$  are lower in the Fornax stars. According to Letarte et al. (2010), the derived Ca and Ti abundances may, however, be affected by non-LTE effects. Spurious offsets may also arise when comparing abundances for two samples of stars with different sets of atmospheric parameters, i.e. red giants in dSph galaxies and dwarf stars in the solar neighborhood.

As seen from Fig. 7,  $[\text{Na}/\text{Fe}]$  and  $[\text{Ni}/\text{Fe}]$  in Fornax extend the correlation defined by the solar neighborhood stars to lower values of  $[\text{Na}/\text{Fe}]$ , albeit with a larger scatter because of the lower precision of the Fornax abundances.  $[\text{Ba}/\text{Y}]$  in Fornax rises sharply with increasing  $[\text{Fe}/\text{H}]$  and reaches  $[\text{Ba}/\text{Y}] \sim 0.8$  at  $[\text{Fe}/\text{H}] = -0.8$ , i.e. much higher than  $[\text{Ba}/\text{Y}]$  for the low- $\alpha$  stars. Thus, Fornax has more extreme abundance anomalies than the low- $\alpha$  population. This may be related to differences in the SFR; the majority of stars in Fornax have ages between 2 and 6 Gyr (Letarte et al. 2010), whereas the low- $\alpha$  stars have ages around 10 Gyr (Schuster et al., in preparation).

Mn, Cu, and Zn were not included in the Fornax study by Letarte et al. (2010). Sagittarius is the only dSph for which these

elements have been studied in some detail and the data refer mainly to the metallicity range  $-0.5 < [\text{Fe}/\text{H}] < 0.0$ .  $[\text{Mn}/\text{Fe}]$  falls below the trend for Galactic disk stars (McWilliam et al. 2003), and both  $[\text{Cu}/\text{Fe}]$  and  $[\text{Zn}/\text{Fe}]$  are even lower than in the low- $\alpha$  population (McWilliam & Smecker-Hane 2005; Sbordone et al. 2007). Again, one may speculate that these extreme abundance anomalies are connected to a very prolonged star formation history of Sagittarius.

It is also interesting to compare the abundance ratios in low- $\alpha$  stars with ratios obtained for irregular galaxies. Kaufer et al. (2004) analyzed three A-type supergiants in the dwarf Irr galaxy Sextans A and found  $[\alpha/\text{Fe}] \sim -0.1$  at  $[\text{Fe}/\text{H}] = -1.0$ . The same low value of  $[\alpha/\text{Fe}]$  was obtained for three M-type supergiants with  $[\text{Fe}/\text{H}] \simeq -0.7$  in the dIrr galaxy IC 1613 by Tautvaišienė et al. (2007). Hence,  $[\alpha/\text{Fe}]$  in these dIrr galaxies is about 0.2 dex lower than the ratio for low- $\alpha$  halo stars.

Finally, there are some similarities between abundance ratios in low- $\alpha$  halo stars and ratios obtained by Pompéia et al. (2008) for RGB stars belonging to the inner disk of the Large Magellanic Cloud (LMC). The trends of  $[\text{Mg}/\text{Fe}]$ ,  $[\text{Si}/\text{Fe}]$ , and  $[\text{Ti}/\text{Fe}]$  as a function of  $[\text{Fe}/\text{H}]$  are about the same except that metallicities as high as  $[\text{Fe}/\text{H}] \sim -0.4$  are reached in LMC.  $[\text{Na}/\text{Fe}]$  and  $[\text{Ni}/\text{Fe}]$  are negative in the LMC stars, similar to the low- $\alpha$  stars, but the correlation between these ratios is not so clear as in Fig. 7 (see Fig. 14 in Pompéia et al. 2008). Furthermore, underabundances of  $[\text{Cu}/\text{Fe}]$  are observed both in the LMC and in the low- $\alpha$  population. However, there also are differences; the LMC stars have lower  $[\text{Ca}/\text{Fe}]$ , and  $[\text{Ba}/\text{Y}]$  shows a much steeper increase with  $[\text{Fe}/\text{H}]$  than found for the low- $\alpha$  stars.

### 3.4. Comparison with $\omega$ Cen

As mentioned in Sect. 1, the majority of low- $\alpha$  stars move on retrograde orbits close to the Galactic plane with a wide distribution of the  $U$ -velocity component. This resembles the orbital characteristics of stars captured from a satellite galaxy that is dragged into the Galactic plane by dynamical friction (Meza et al. 2005). Given that the  $\omega$  Cen globular cluster is probably the nucleus of a dwarf galaxy (e.g. Bekki & Freeman 2003), and that many of the low- $\alpha$  stars have a  $V$ -velocity component similar to that of  $\omega$  Cen, it is possible that a significant fraction of the low- $\alpha$  halo stars in the solar neighborhood have been formed in the  $\omega$  Cen progenitor galaxy. Hence, it is of interest to compare abundance ratios in the low- $\alpha$  stars with the corresponding ratios in  $\omega$  Cen stars.

$\omega$  Cen is unique among globular clusters by having a wide metallicity distribution. In a comprehensive, high-resolution study of 855 red giants in  $\omega$  Cen, i.e. essentially all stars brighter than  $V = 13.5$ , Johnson & Pilachowski (2010) identified four peaks in the metallicity distribution at  $[\text{Fe}/\text{H}] \simeq -1.75$ ,  $-1.50$ ,  $-1.10$ , and  $-0.75$ . A Gaussian decomposition of the distribution (see Fig. 8 in Johnson & Pilachowski 2010) indicates a corresponding frequency distribution of 61 %, 27 %, 10 %, and 2 %, for the stars in  $\omega$  Cen. The upper limit of  $[\text{Fe}/\text{H}]$  in  $\omega$  Cen corresponds quite well to that of the low- $\alpha$  stars, but there are too few metal-rich stars in  $\omega$  Cen to match the  $[\text{Fe}/\text{H}]$  distribution for the low- $\alpha$  stars.

Regarding the trend of  $[\alpha/\text{Fe}]$  vs.  $[\text{Fe}/\text{H}]$  in  $\omega$  Cen, there are conflicting results. From high-resolution spectroscopy of six red giants, Pancino et al. (2002) found evidence of a decline of  $[\text{Si}/\text{Fe}]$  and  $[\text{Ca}/\text{Fe}]$  starting around  $[\text{Fe}/\text{H}] \sim -1$ . A similar decline in  $[\alpha/\text{Fe}]$  ( $\alpha \equiv \text{O, Mg, Si, and Ca}$ ) was found by Origlia et al. (2003) on the basis of medium-resolution IR spectra of 21

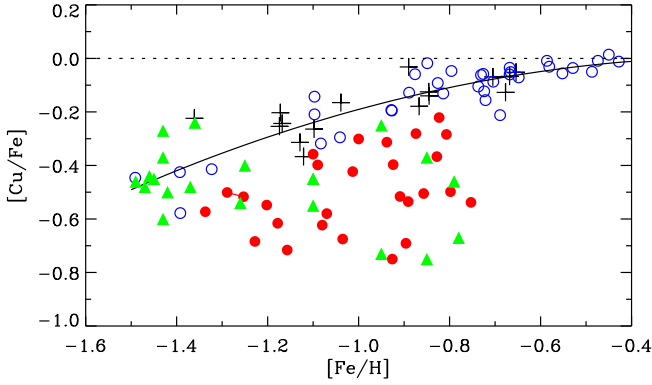


**Fig. 8.**  $[\text{Cu}/\text{Fe}]$  vs.  $[\text{Fe}/\text{H}]$ . Stars in this paper are shown with the same symbols as in Fig. 2. The solid line is a quadratic fit to the  $[\text{Cu}/\text{Fe}]$  -  $[\text{Fe}/\text{H}]$  trend for thick-disk and high- $\alpha$  halo stars. Green triangles show values for RGB stars in the  $\omega$  Cen globular cluster (Cunha et al. 2002).

giants in  $\omega$  Cen. The extensive high-resolution study of Johnson & Pilachowski (2010), which includes more than 70 stars in the metallicity range  $-1.2 < [\text{Fe}/\text{H}] < -0.7$ , indicates, however, that  $[\text{Si}/\text{Fe}]$ ,  $[\text{Ca}/\text{Fe}]$ , and  $[\text{Ti}/\text{Fe}]$  are essentially constant at a level of  $+0.3$  to  $+0.4$  dex suggesting that SNe Ia have not contributed to the chemical enrichment in  $\omega$  Cen. Even if one believes in the results of Pancino et al. (2002) and Origlia et al. (2003), it is clear that the contribution of SNe Ia started at a higher metallicity ( $[\text{Fe}/\text{H}]_{\text{knee}} \approx -1$ ) than in the case of the present low- $\alpha$  population ( $[\text{Fe}/\text{H}]_{\text{knee}} \lesssim -1.5$ ).

$[\text{Na}/\text{Fe}]$  is very different in low- $\alpha$  and  $\omega$  Cen stars. Instead of being negative,  $[\text{Na}/\text{Fe}]$  is positive in  $\omega$  Cen stars with  $[\text{Fe}/\text{H}] > -1.4$ , and there is a clear Na-O anti-correlation (Johnson & Pilachowski 2010) as found in all well-studied globular clusters (Carretta et al. 2009). This anti-correlation may be ascribed to the CNO and Ne-Na cycles in connection with hydrogen burning in intermediate-mass AGB stars (Ventura et al. 2001). According to hydrodynamical simulations by D’Ercole et al. (2008), the gas ejected from such AGB stars collects in the cluster core, which could explain the difference in  $[\text{Na}/\text{Fe}]$  between stars remaining in  $\omega$  Cen itself and those originating from the progenitor galaxy.

Turning to the iron-peak elements, there are some similarities between  $\omega$  Cen and the low- $\alpha$  halo population. As noted by Johnson & Pilachowski (2010),  $[\text{Ni}/\text{Fe}]$  in  $\omega$  Cen decreases slightly at  $[\text{Fe}/\text{H}] > -1.3$ . From data in their Table 5, an average  $\langle [\text{Ni}/\text{Fe}] \rangle = -0.11$  is obtained for 42 stars with  $-1.1 \leq [\text{Fe}/\text{H}] < -0.7$ , which compares well with the corresponding value  $\langle [\text{Ni}/\text{Fe}] \rangle = -0.13$  for 21 low- $\alpha$  stars. As shown in Fig. 8, there is also a striking agreement between  $[\text{Cu}/\text{Fe}]$  in low- $\alpha$  stars and the ratios determined for red giants in  $\omega$  Cen by Cunha et al. (2002). Recently, Cunha et al. (2010) have also determined Mn abundances in ten RGB stars in  $\omega$  Cen covering the metallicity range  $-1.8 < [\text{Fe}/\text{H}] < -0.9$ . Eight stars have  $[\text{Mn}/\text{Fe}]$  values overlapping the trend for the solar neighborhood stars, but the two most metal-rich stars with  $[\text{Fe}/\text{H}] \approx -1.2$  and  $-0.9$  have  $[\text{Mn}/\text{Fe}] \approx -0.9$ , i.e. far below the values for the high- and low- $\alpha$  halo stars. More data on Mn abundances in  $\omega$  Cen are needed to confirm, analyze, and understand this puzzling deviation.

Abundances of neutron capture elements in  $\omega$  Cen were determined for ten RGB stars having  $-1.8 < [\text{Fe}/\text{H}] < -0.8$  by Smith et al. (2000). In this metallicity range, the abundances of the heavy- $s$  elements, Ba and La, increase by more than 1 dex relative to Fe.  $[\text{Y}/\text{Fe}]$  shows a much smaller increase, i.e. less

than 0.3 dex. Hence, the  $\omega$  Cen stars show a much more dramatic increase in  $[\text{Ba}/\text{Y}]$  with  $[\text{Fe}/\text{H}]$  than the low- $\alpha$  stars. The reason for this difference could be that winds from low-mass AGB stars producing the  $s$ -process elements are more efficiently retained in the cluster than the faster moving Type II ejecta (Smith et al. 2000). These authors also suggest that all elements produced by Type Ia SNe escape from the  $\omega$  Cen cluster, which would explain the ‘high’ trend of  $[\alpha/\text{Fe}]$  found by Johnson & Pilachowski (2010).

As seen from this discussion, only  $[\text{Ni}/\text{Fe}]$  and  $[\text{Cu}/\text{Fe}]$  agree between the stars in the  $\omega$  Cen cluster and those in the low- $\alpha$  population. There are large differences in the distributions of  $[\alpha/\text{Fe}]$ ,  $[\text{Na}/\text{Fe}]$ , and  $[\text{Ba}/\text{Y}]$ . Hence, if some of the low- $\alpha$  stars were accreted from  $\omega$  Cen, the chemical evolution pattern must have been different in the inner and outer parts of the progenitor galaxy. Evidence of such a scenario comes from the recent work by Chou et al. (2010) on abundances in the Sagittarius dSph galaxy; stars in the leading north arm tend to have lower values of  $[\text{La}/\text{Y}]$  than stars in the Sgr core for the metallicity range  $-1 < [\text{Fe}/\text{H}] < 0$  (see Fig. 6 in the Chou et al. paper).

#### 4. Conclusions

In this paper very precise abundances of Mn, Cu, Zn, Y, and Ba have been determined relative to Fe for stars in the solar neighborhood with halo kinematics. The two populations, high- and low- $\alpha$  stars, that were found to have different ratios of  $[\alpha/\text{Fe}]$ ,  $[\text{Na}/\text{Fe}]$ , and  $[\text{Ni}/\text{Fe}]$  in our first paper (NS10) are also separated in  $[\text{Cu}/\text{Fe}]$ ,  $[\text{Zn}/\text{Fe}]$ , and  $[\text{Ba}/\text{Y}]$ . There is, however, no significant differences in  $[\text{Mn}/\text{Fe}]$ .

Trends and correlations between the abundance ratios may to a large extent be explained from existing nucleosynthesis calculations if the high- $\alpha$  stars have been formed in regions with such a high SFR that only massive stars and SNe II have contributed to the chemical evolution up to  $[\text{Fe}/\text{H}] \approx -0.4$ . The low- $\alpha$  stars, on the other hand, may originate from systems with a slower chemical evolution, characterized by delayed enrichment from relatively metal-poor SNe Ia and low-mass AGB stars in addition to the contributions from massive stars and Type II SNe. It is, however, difficult to explain that there is no significant difference in  $[\text{Mn}/\text{Fe}]$  between the high- and low- $\alpha$  populations. Furthermore, the data for  $[\text{Ni}/\text{Fe}]$  call for a revision of the Ni yields from SNe Ia.

RGB stars in present-day dSph satellite galaxies show abundance trends of  $[\alpha/\text{Fe}]$ ,  $[\text{Na}/\text{Fe}]$ ,  $[\text{Ni}/\text{Fe}]$ ,  $[\text{Cu}/\text{Fe}]$ , and  $[\text{Ba}/\text{Y}]$  that have some similarities with the trends for the low- $\alpha$  population, but there is no exact matching. In general, existing dSph galaxies seem to be characterized by an even slower chemical evolution than the systems in which the low- $\alpha$  stars were formed.

As discussed in NS10, the kinematics of the low- $\alpha$  stars suggest that some of them were accreted from the progenitor galaxy of the  $\omega$  Cen globular cluster. We have looked for supporting evidence from chemical abundance ratios, but have found more differences between the  $\omega$  Cen cluster and the low- $\alpha$  stars than similarities. The distributions of  $[\text{Ni}/\text{Fe}]$  and  $[\text{Cu}/\text{Fe}]$  for RGB stars in  $\omega$  Cen overlap well with those of the low- $\alpha$  population, but  $[\text{Na}/\text{Fe}]$  and  $[\text{Ba}/\text{Y}]$  are very different in  $\omega$  Cen and low- $\alpha$  stars. This difference could be explained if the products of AGB stars are selectively retained within the  $\omega$  Cen cluster. The trend of  $[\alpha/\text{Fe}]$  is also different for  $\omega$  Cen and the low- $\alpha$  population, so one has to invoke differential loss of SNe II and SNe Ia winds from  $\omega$  Cen if some of the low- $\alpha$  stars did originate from the progenitor galaxy.

Zolotov et al. (2009, 2010) have recently used N-body and smooth particle hydrodynamic simulations to investigate the kinematics and  $[\alpha/\text{Fe}]$  trends of stellar halos of large galaxies similar to the Milky Way. They find that the inner halos ( $R < 20 \text{ kpc}$ ) contain both accreted and in situ formed stars. These two populations are separated in  $[\alpha/\text{Fe}]$  at the high end of the metallicity distribution function if the halo was formed in connection with a few major mergers ( $M_{\text{satellite}}/M_{\text{primary}} > 0.1$ ) at early times, i.e. more than  $8 - 9 \text{ Gyr}$  ago. The in situ halo stars formed in the innermost  $\sim 4 \text{ kpc}$  of the galaxy in a deep potential well causing the SFR to be so high that only core collapse SNe contributed to the chemical enrichment. Later these stars were ‘heated’ to halo kinematics by mergers. The accreted stars, on the other hand, formed in satellite galaxies with shallower potential wells and hence lower SFR allowing SNe Ia to contribute to the enrichment at the high end of the metallicity distribution.

The dual distribution of  $[\alpha/\text{Fe}]$  obtained in the simulations of Zolotov et al. (2010) corresponds qualitatively to the abundance trends determined in NS10 and in this paper. Thus, the high- $\alpha$  population may consist of stars formed in the innermost part of the Milky Way and displaced to the halo by mergers, whereas the low- $\alpha$  stars may have been accreted at early times from a few, relatively massive satellite galaxies. The dispersion in abundance ratios at a given  $[\text{Fe}/\text{H}]$  suggests that these satellites followed somewhat different chemical evolution patterns. Present-day dSph galaxies are less massive, which may explain that they have more extreme abundance anomalies than the low- $\alpha$  stars. Clearly, this scenario should be tested by determining  $[\alpha/\text{Fe}]$  and other abundance ratios for a large sample of halo stars situated in other regions than the solar neighborhood.

*Acknowledgements.* This publication made use of the SIMBAD database operated at CDS, Strasbourg, France, and NASA’s Astrophysics Data System. The staff at the Nordic Optical Telescope is thanked for competent assistance in obtaining spectra for this project.

## References

- Anstee, S.D., & O’Mara, B.J. 1995, *MNRAS*, 276, 859  
 Asplund, M. 2005, *ARA&A*, 43, 481  
 Badenes, C., Bravo, E., & Hughes, J.P. 2008, *ApJ*, 680, L33  
 Barklem, P.S., & O’Mara, B.J. 1997, *MNRAS*, 290, 102  
 Barklem, P.S., Piskunov, N., & O’Mara, B.J. 2000, *A&AS*, 142, 467  
 Bekki, K., & Freeman, K.C. 2003, *MNRAS*, 346, L11  
 Bensby, T., Feltzing, S., Lundström, I., & Ilyin, I. 2005, *A&A*, 433, 185  
 Bergemann, M., & Gehren, T. 2007, *A&A*, 473, 291  
 Bergemann, M., & Gehren, T. 2008, *A&A*, 492, 823  
 Bisterzo, S., Gallino, R., Pignatari, M., et al. 2004, *Mem.S.A.It.*, 75, 741  
 Busso, M., Gallino, R., & Wasserburg, G.J. 1999, *ARA&A*, 37, 239  
 Carretta, E., Bragaglia, A., Gratton, R., & Lucatello, S. 2009, *A&A*, 505, 139  
 Carretta, E., Bragaglia, A., Gratton, R., et al. 2010, *A&A*, 520, A95  
 Cescutti, G., Matteucci, F., Lanfranchi, G.A., & McWilliam, A. 2008, *A&A*, 491, 401  
 Chou, M.-Y., Cunha, K., Majewski, S.R., et al. 2010, *ApJ*, 708, 1290  
 Chou, M.-Y., Majewski, S.R., Cunha, K., et al. 2007, *ApJ*, 670, 346  
 Cohen, J.G., & Huang, W. 2009, *ApJ*, 701, 1053  
 Cohen, J.G., & Huang, W. 2010, *ApJ*, 719, 931  
 Collet, R., Asplund, M., & Nissen, P.E. 2009, *PASA*, 26, 330  
 Cunha, K., Smith, V.V., Bergemann, M., Suntzeff, N.B., & Lambert, D.L. 2010, *ApJ*, 717, 333  
 Cunha, K., Smith, V.V., Suntzeff, N.B., et al. 2002, *AJ*, 124, 379  
 D’Ercole, A., Vesperini, E., D’Antona, F., McMillan, S.L.W., & Recchi, S. 2008, *MNRAS*, 391, 825  
 Dinescu, D.I., Girard, T.M., & van Altena, W.F. 1999, *AJ*, 117, 1792  
 Feltzing, S., Fohlman, M., & Bensby, T. 2007, *A&A*, 467, 665  
 Fenner, Y., Gibson, B.K., Gallino, R., & Lugaro, M. 2006, *ApJ*, 646, 184  
 Freeman, K., & Bland-Hawthorn, J. 2002, *ARA&A*, 40, 487  
 Fulbright, J.P. 2002, *AJ*, 123, 404  
 Gratton, R.G. 1989, *A&A*, 208, 171  
 Gratton, R.G., Carretta, E., Desidera, S., et al. 2003, *A&A*, 406, 131  
 Gustafsson, B., Edvardsson, B., Eriksson, K., et al. 2008, *A&A*, 486, 951  
 Hannaford, P., Lowe, R.M., Grevesse, N., Biémont, E., & Whaling, W. 1982, *ApJ*, 261, 736  
 Helmi, A. 2008, *A&ARv*, 15, 145  
 Ishigaki, M., Chiba, M., & Aoki, W. 2010, *PASJ*, 62, 143  
 Johnson, C.I., & Pilachowski, C.A. 2010, *ApJ*, 722, 1373  
 Jonsell, K., Edvardsson, B., Gustafsson, B. et al. 2005, *A&A*, 440, 321  
 Kaufer, A., Venn, K.A., Tolstoy, E., Pinte, C., & Kudritzki, R.-P. 2004, *AJ*, 127, 2723  
 Keller, S.C., Yong, D., & Da Costa, G.S. 2010, *ApJ*, 720, 940  
 Klement, R.J. 2010, *A&ARv*, 18, 567  
 Kobayashi, C., & Nomoto, K. 2009, *ApJ*, 707, 1466  
 Kobayashi, C., Umeda, H., Nomoto, K., Tominaga, N., & Ohkubo, T. 2006, *ApJ*, 653, 1145  
 Koch, A., Grebel, E.K., Gilmore, G.F., et al. 2008, *AJ*, 135, 1580  
 Korn, A.J., Grundahl, F., Richard, O., et al. 2007, *ApJ*, 671, 402  
 Kurucz, R.L., Furenlid, I., Brault, J., & Testerman, L. 1984, *Solar Flux Atlas from 296 to 1300 nm*, National Solar Observatory, Sunspot, New Mexico  
 Lanfranchi, G.A., & Matteucci, F. 2003, *MNRAS*, 345, 71  
 Latham, D.W., Stefanik, R.P., Torres, G., et al. 2002, *AJ*, 124, 1144  
 Letarte, B., Hill, V., Tolstoy, E., et al. 2010, *A&A*, 523, A17  
 Maoz, D., Mannucci, F., Li, W., et al. 2010, *arXiv:1002.3056*  
 McWilliam, A. 1998, *AJ*, 115, 1640  
 McWilliam, A., Rich, R.M., & Smecker-Hane, T.A. 2003, *ApJ*, 592, L21  
 McWilliam, A., & Smecker-Hane, T.A. 2005, *ApJ*, 622, L29  
 Meza, A., Navarro, J.F., Abadi, M.G., & Steinmetz, M. 2005, *MNRAS*, 359, 93  
 Nissen, P.E., Akerman, C., Asplund, M., et al. 2007, *A&A*, 469, 319  
 Nissen, P.E., & Schuster, W.J. 1997, *A&A*, 326, 751  
 Nissen, P.E., & Schuster, W.J. 2010, *A&A*, 511, L10 (NS10)  
 Nomoto, K., Iwamoto, K., Nakasato, N., et al. 1997, *Nucl. Phys. A*, 621, 467  
 Origlia, L., Ferraro, F.R., Bellazzini, M., & Pancino, E. 2003, *ApJ*, 591, 916  
 Pancino, E., Pasquini, L., Hill, V., Ferraro, F.R., & Bellazzini, M. 2002, *ApJ*, 568, L101  
 Pompéia, L., Hill, V., Spite, M., et al. 2008, *A&A*, 480, 379  
 Prochaska, J.X., Naumov, S.O., Carney, B.W., McWilliam, A., & Wolfe, A.M. 2000, *AJ*, 120, 2513  
 Purcell, C.W., Bullock, J.S., & Kazantzidis, S. 2010, *MNRAS*, 404, 1711  
 Qu, Y., Di Matteo, P., Lehnert, M.D., & van Driel, W. 2011, *arXiv:1102.1879*  
 Sbordone, L., Bonifacio, P., Buonanno, R., et al. 2007, *A&A*, 465, 815  
 Schaller, G., Schaerer, D., Meynet, G., & Maeder, A. 1992, *A&AS*, 96, 269  
 Schuster, W.J., Moitinho, A., Márquez, A., Parrao, L., & Covarrubias, E. 2006, *A&A*, 445, 939  
 Smith, V.V., Suntzeff, N.B., Cunha, K., et al. 2000, *AJ*, 119, 1239  
 Sneden, C., Gratton, R.G., & Crocker, D.A. 1991, *A&A*, 246, 354  
 Stephens, A., & Boesgaard, A.M. 2002, *AJ*, 123, 1647  
 Takeda, Y., Hashimoto, O., Taguchi, H., et al. 2005, *PASJ*, 57, 751  
 Takeda, Y., & Takada-Hidai, M. 2010, *arXiv:1009.0824*  
 Tautvaišienė, G., Geisler, D., Wallerstein, G., et al. 2007, *AJ*, 134, 2318  
 Tinsley, B.M. 1979, *ApJ*, 229, 1046  
 Tolstoy, E., Hill, V., & Tosi, M. 2009, *ARA&A*, 47, 371  
 Travaglio, C., Gallino, R., Arnone, E., et al. 2004, *ApJ*, 601, 864  
 Tsujimoto, T., Nomoto, K., Yoshii, Y., et al. 1995, *MNRAS*, 277, 945  
 Unsöld, A. 1955, *Physik der Sternatmosphären*, Springer Verlag, Berlin  
 Venn, K.A., Irwin, M., Shetrone, M.D., et al. 2004, *AJ*, 128, 1177  
 Ventura, P., D’Antona, F., Mazzitelli, I., & Gratton, R. 2001, *ApJ*, 550, L65  
 Woosley, S.E., & Weaver, T.A. 1995, *ApJS*, 101, 181  
 Zolotov, A., Willman, B., Brooks, A.M., et al. 2009, *ApJ*, 702, 1058  
 Zolotov, A., Willman, B., Brooks, A.M., et al. 2010, *ApJ*, 721, 738

**Table 1.** Atmospheric parameters and abundance ratios for stars with VLT/UVES spectra.

ID	$T_{\text{eff}}$ (K)	$\log g$	[Fe/H]	[ $\alpha$ /Fe]	[Mn/Fe]	[Cu/Fe]	[Zn/Fe]	[Y/Fe]	[Ba/Fe]	Class <sup>a</sup>
BD-21 3420	5808	4.26	-1.13	0.31	-0.32	-0.31	0.17	0.11	0.02	TD
CD-33 3337	5979	3.86	-1.36	0.30	-0.27	-0.22	0.10	-0.06	-0.19	TD
CD-43 6810	5945	4.26	-0.43	0.23	-0.19	-0.01	0.18	0.23	-0.08	high- $\alpha$
CD-45 3283	5597	4.55	-0.91	0.12	-0.31	-0.52	-0.03	-0.20	-0.14	low- $\alpha$
CD-51 4628	6153	4.31	-1.30	0.22	-0.36		0.00	-0.11	-0.16	low- $\alpha$
CD-57 1633	5873	4.28	-0.90	0.07	-0.34	-0.69	-0.10	-0.27	-0.14	low- $\alpha$
CD-61 282	5759	4.31	-1.23	0.22	-0.37	-0.68	0.05	-0.16	-0.24	low- $\alpha$
G05-19	5854	4.26	-1.18	0.19	-0.35	-0.62	0.01	-0.12	-0.17	low- $\alpha$
G05-40	5795	4.17	-0.81	0.31	-0.27	-0.13	0.18	0.06	0.00	high- $\alpha$
G18-28	5372	4.41	-0.83	0.31	-0.22	-0.09	0.17	0.04	-0.07	high- $\alpha$
G18-39	6040	4.21	-1.39	0.34	-0.36	-0.58	0.19	0.12	-0.02	high- $\alpha$
G20-15	6027	4.32	-1.49	0.24	-0.32		0.11	-0.14	-0.22	(low- $\alpha$ )
G46-31	5901	4.23	-0.83	0.15	-0.29	-0.37	-0.03	-0.05	-0.08	low- $\alpha$
G63-26	6043	4.18	-1.56	0.37	-0.32		0.16	0.17	0.11	(high- $\alpha$ )
G66-22	5236	4.41	-0.86	0.12	-0.28	-0.50	-0.05	-0.16	-0.10	low- $\alpha$
G82-05	5277	4.45	-0.75	0.09	-0.28	-0.54	-0.08	-0.19	-0.10	low- $\alpha$
G112-43	6074	4.03	-1.25	0.24	-0.19	-0.52	0.30	-0.14	-0.27	low- $\alpha$
G112-44	5819	4.25	-1.29	0.22	-0.23	-0.50	0.28	-0.25	-0.29	low- $\alpha$
G114-42	5643	4.38	-1.10	0.19	-0.30	-0.36	0.02	-0.14	-0.18	low- $\alpha$
G121-12	5928	4.23	-0.93	0.10	-0.33	-0.75	-0.12	-0.17	-0.14	low- $\alpha$
G159-50	5624	4.37	-0.93	0.31	-0.25	-0.19	0.14	0.05	-0.01	high- $\alpha$
G188-22	5974	4.18	-1.32	0.35	-0.34	-0.41	0.15	0.15	0.03	high- $\alpha$
HD3567	6051	4.02	-1.16	0.21	-0.33	-0.72	0.01	-0.05	-0.09	low- $\alpha$
HD17820	5773	4.22	-0.67	0.29	-0.19	-0.07	0.14	-0.11	-0.23	TD
HD22879	5759	4.25	-0.85	0.31	-0.27	-0.14	0.14	0.01	-0.12	TD
HD25704	5868	4.26	-0.85	0.24	-0.22	-0.13	0.07	-0.13	-0.22	TD
HD51754	5767	4.29	-0.58	0.26	-0.17	-0.03	0.14	-0.15	-0.23	high- $\alpha$
HD59392	6012	3.91	-1.60	0.32	-0.36		0.14	0.13	-0.07	(low- $\alpha$ )
HD76932	5877	4.13	-0.87	0.29	-0.25	-0.18	0.10	0.03	-0.07	TD
HD97320	6008	4.19	-1.17	0.28	-0.24	-0.24	0.09	-0.09	-0.19	TD
HD103723	5938	4.19	-0.80	0.14	-0.32	-0.50	-0.07	-0.16	-0.11	low- $\alpha$
HD105004	5754	4.30	-0.82	0.14	-0.21	-0.22	0.04	-0.15	-0.16	low- $\alpha$
HD106516	6196	4.42	-0.68	0.29	-0.23	-0.13	0.18	-0.05	-0.18	TD
HD111980	5778	3.96	-1.08	0.34	-0.34	-0.32	0.15	0.16	0.07	high- $\alpha$
HD113679	5672	3.99	-0.65	0.32	-0.23	-0.07	0.17	-0.01	-0.17	high- $\alpha$
HD114762A	5856	4.21	-0.70	0.24	-0.19	-0.07	0.10	-0.16	-0.25	TD
HD120559	5412	4.50	-0.89	0.30	-0.17	-0.03	0.16	-0.08	-0.22	TD
HD121004	5669	4.37	-0.70	0.32	-0.22	-0.09	0.14	0.04	-0.12	high- $\alpha$
HD126681	5507	4.45	-1.17	0.35	-0.32	-0.25	0.15	0.23	0.14	TD
HD132475	5646	3.76	-1.49	0.38	-0.36	-0.45	0.19	0.19	0.06	(high- $\alpha$ )
HD148816	5823	4.13	-0.73	0.27	-0.21	-0.06	0.19	-0.15	-0.26	high- $\alpha$
HD163810	5501	4.56	-1.20	0.21	-0.30	-0.55	0.02	-0.11	-0.16	low- $\alpha$
HD175179	5713	4.33	-0.65	0.29	-0.23	-0.05	0.18	0.13	0.12	TD
HD179626	5850	4.13	-1.04	0.31	-0.28	-0.29	0.05	0.01	-0.17	high- $\alpha$
HD189558	5617	3.80	-1.12	0.33	-0.34	-0.37	0.11	0.18	0.10	TD
HD193901	5656	4.36	-1.09	0.16	-0.34	-0.62	-0.03	-0.20	-0.19	low- $\alpha$
HD194598	5942	4.33	-1.09	0.18	-0.25	-0.40	0.03	-0.13	-0.20	low- $\alpha$
HD199289	5810	4.28	-1.04	0.30	-0.26	-0.17	0.13	-0.09	-0.21	TD
HD205650	5698	4.32	-1.17	0.30	-0.28	-0.20	0.14	-0.04	-0.19	TD
HD219617 <sup>b</sup>	5862	4.28	-1.45	0.28	-0.34		0.09	-0.25	-0.28	(low- $\alpha$ )
HD222766	5334	4.27	-0.67	0.30	-0.24	-0.06	0.21	-0.01	-0.09	high- $\alpha$
HD241253	5831	4.31	-1.10	0.29	-0.31	-0.26	0.14	0.07	-0.04	TD
HD284248	6135	4.25	-1.57	0.27	-0.33		0.09	-0.20	-0.31	(low- $\alpha$ )

<sup>a</sup> Classification as thick disk (TD), low- $\alpha$ , or high- $\alpha$ . For halo stars with [Fe/H] < -1.4, the classification is uncertain and given in parentheses.<sup>b</sup> As noted by Takeda & Takada-Hidai (2010), HD 219617 is a double star comprising  $V = 8.77$  and 9.08 mag. components with a separation of 0.8 arcsec and nearly identical spectra. The UVES spectrum, obtained with a 0.8 arcsec slit under rather poor seeing conditions, is an unspecified average of the two spectra.

**Table 2.** Atmospheric parameters and abundance ratios for stars with NOT/FIES spectra.

ID	$T_{\text{eff}}$ (K)	$\log g$	[Fe/H]	[ $\alpha$ /Fe]	[Mn/Fe]	[Cu/Fe]	[Zn/Fe]	[Y/Fe]	[Ba/Fe]	Class <sup>a</sup>
G05-36	6013	4.23	-1.23	0.35	-0.38		0.12	0.16	0.09	high- $\alpha$
G13-38	5263	4.54	-0.88	0.32	-0.21	-0.06	0.21	0.08	-0.06	high- $\alpha$
G15-23	5297	4.57	-1.10	0.34	-0.32	-0.14	0.22	0.38	0.25	high- $\alpha$
G16-20	5625	3.64	-1.42	0.26	-0.34		0.09	-0.13	-0.22	(low- $\alpha$ )
G20-15 <sup>b</sup>	6072	4.36	-1.41	0.21	-0.33		0.09	-0.09	-0.16	(low- $\alpha$ )
G21-22	5901	4.24	-1.09	0.09	-0.39		-0.09	-0.33	-0.34	low- $\alpha$
G24-13	5673	4.31	-0.72	0.29	-0.25	-0.16	0.21	-0.01	-0.09	high- $\alpha$
G24-25 <sup>c</sup>	5828	3.86	-1.40	0.35	-0.37		0.22	0.82	1.45	(high- $\alpha$ )
G31-55	5638	4.30	-1.10	0.29	-0.26	-0.21	0.11	-0.02	-0.15	high- $\alpha$
G49-19	5772	4.25	-0.55	0.27	-0.19	-0.06	0.18	-0.15	-0.19	high- $\alpha$
G53-41	5859	4.27	-1.20	0.23	-0.38		0.03	0.05	0.24	low- $\alpha$
G56-30	5830	4.26	-0.89	0.11	-0.32	-0.54	-0.12	-0.27	-0.19	low- $\alpha$
G56-36	5933	4.28	-0.94	0.20	-0.27	-0.31	0.01	-0.05	-0.02	low- $\alpha$
G57-07	5676	4.25	-0.47	0.31	-0.22	-0.01	0.20	-0.08	-0.13	high- $\alpha$
G74-32	5772	4.36	-0.72	0.30	-0.24	-0.12	0.15	-0.01	-0.16	high- $\alpha$
G75-31	6010	4.02	-1.03	0.20	-0.34	-0.68	-0.03	-0.11	-0.16	low- $\alpha$
G81-02	5859	4.19	-0.69	0.19	-0.24	-0.21	0.06	-0.17	-0.13	high- $\alpha$
G85-13	5628	4.38	-0.59	0.28	-0.20	-0.01	0.21	0.00	-0.07	high- $\alpha$
G87-13	6085	4.13	-1.09	0.20	-0.34	-0.58	-0.03	-0.11	-0.16	low- $\alpha$
G94-49	5373	4.50	-0.80	0.31	-0.19	-0.05	0.21	0.02	-0.14	high- $\alpha$
G96-20 <sup>c</sup>	6293	4.41	-0.89	0.28	-0.28	-0.13	0.11	0.28	0.68	high- $\alpha$
G98-53	5848	4.23	-0.87	0.19	-0.30	-0.28	0.06	-0.06	-0.12	low- $\alpha$
G99-21	5487	4.39	-0.67	0.29	-0.23	-0.04	0.20	-0.03	-0.11	high- $\alpha$
G119-64	6181	4.18	-1.48	0.28	-0.34		0.02	-0.08	-0.23	(low- $\alpha$ )
G125-13	5848	4.28	-1.43	0.27	-0.38		0.05	-0.22	-0.31	(high- $\alpha$ )
G127-26	5791	4.14	-0.53	0.24	-0.20	-0.04	0.21	-0.13	-0.14	high- $\alpha$
G150-40	5968	4.09	-0.81	0.16	-0.20	-0.28	0.01	-0.16	-0.13	low- $\alpha$
G161-73	5986	4.00	-1.00	0.16	-0.36		-0.08	-0.19	-0.11	low- $\alpha$
G170-56	5994	4.12	-0.92	0.17	-0.30	-0.40	-0.04	-0.14	-0.15	low- $\alpha$
G172-61	5225	4.47	-1.00	0.19	-0.26	-0.30	0.09	0.11	-0.05	low- $\alpha$
G176-53	5523	4.48	-1.34	0.18	-0.35	-0.57	0.08	-0.26	-0.26	low- $\alpha$
G180-24	6004	4.21	-1.39	0.33	-0.34	-0.43	0.12	0.07	-0.18	high- $\alpha$
G187-18	5607	4.39	-0.67	0.26	-0.19	-0.05	0.11	-0.16	-0.18	high- $\alpha$
G192-43	6170	4.29	-1.34	0.26	-0.38		0.08	-0.09	-0.17	low- $\alpha$
G232-18	5559	4.48	-0.93	0.32	-0.30	-0.19	0.15	0.08	-0.03	high- $\alpha$
HD148816 <sup>b</sup>	5840	4.14	-0.70	0.26	-0.21	-0.08	0.12	-0.14	-0.28	high- $\alpha$
HD159482	5737	4.31	-0.73	0.30	-0.23	-0.06	0.14	-0.09	-0.23	high- $\alpha$
HD160693	5714	4.27	-0.49	0.19	-0.21	-0.05	0.14	-0.14	-0.09	high- $\alpha$
HD177095	5349	4.39	-0.74	0.31	-0.24	-0.10	0.19	0.06	-0.03	high- $\alpha$
HD179626 <sup>b</sup>	5855	4.19	-1.00	0.32	-0.31	-0.23	0.08	0.06	-0.14	high- $\alpha$
HD189558 <sup>b</sup>	5623	3.81	-1.12	0.35	-0.32	-0.36	0.13	0.18	0.08	TD
HD193901 <sup>b</sup>	5676	4.41	-1.07	0.17	-0.34	-0.61	0.00	-0.23	-0.24	low- $\alpha$
HD194598 <sup>b</sup>	5926	4.32	-1.08	0.20	-0.28	-0.36	0.01	-0.14	-0.20	low- $\alpha$
HD230409	5318	4.54	-0.85	0.27	-0.16	-0.02	0.16	-0.08	-0.17	high- $\alpha$
HD233511	6006	4.23	-1.55	0.34	-0.44		0.09	-0.18	-0.27	(high- $\alpha$ )
HD237822	5603	4.33	-0.45	0.29	-0.16	0.01	0.22	-0.12	-0.21	high- $\alpha$
HD250792A	5489	4.47	-1.01	0.24	-0.24	-0.42	0.03	-0.12	-0.14	low- $\alpha$

<sup>a</sup> Classification as thick disk (TD), low- $\alpha$ , or high- $\alpha$ . For halo stars with [Fe/H] < -1.4, the classification is uncertain and given in parentheses.<sup>b</sup> Data are also available from UVES spectra (see Table 1).<sup>c</sup> *s*-process enhanced star.

**Table 3.** Line data and equivalent widths measured for the two standard stars (HD 22879 and HD 76932), the solar flux, and the prototypes of low-, and high- $\alpha$  stars, CD -45 3283 and G 159-50.

Element	wavelength [Å]	exc.pot. [eV]	$\log(gf)^a$	HD 22879 EW [mÅ]	HD 76932 EW [mÅ]	solar flux EW [mÅ]	CD -45 3283 EW [mÅ]	G 159-50 EW [mÅ]	etc.
Na I	4982.82	2.10	-1.00	25.4	22.1		9.9	21.5	...
Na I	5682.64	2.10	-0.77	38.2	35.3		19.4	34.2	...
Na I	5688.21	2.10	-0.48	59.8	55.8		32.5	54.1	...
Na I	6154.22	2.10	-1.59	7.4	7.6	37.8	3.6	7.1	...
Na I	6160.74	2.10	-1.30	14.0	13.2	56.9	5.4	11.8	...
Mg I	4730.03	4.34	-2.33						...
Mg I	5711.09	4.34	-1.74	71.0	66.4	115.5	55.9	76.2	...
Si I	5684.48	4.95	-1.68	27.6	26.0	60.7	18.6	26.3	...
Si I	5690.42	4.93	-1.88	20.4	18.2	54.6	13.6	18.5	...
Si I	5701.10	4.93	-2.06	14.1	13.0	40.3	9.6	13.8	...
Si I	6142.48	5.62	-1.52	11.2	11.4	34.6	7.4	10.0	...
Si I	6145.01	5.61	-1.46	13.6	12.5	38.6	9.9	12.5	...
Si I	6155.13	5.62	-0.89	39.5	36.6		26.4	35.1	...
Si I	6237.32	5.61	-1.15	24.3	23.8		14.6	21.6	...
Si I	6243.81	5.61	-1.33	17.3	16.8	46.8	10.2	16.2	...
Si I	6244.47	5.61	-1.36	16.7	15.5	45.3	9.3	15.3	...
Si I	6414.98	5.87	-1.08	18.0	15.3	48.3	11.2	17.4	...
Ca I	5260.38	2.52	-1.79	10.5	9.8	32.1	9.6	11.2	...
Ca I	5349.46	2.71	-0.45	63.1	60.9		61.9		...
Ca I	5512.98	2.93	-0.52	47.9	45.1		45.2	49.5	...
Ca I	5581.97	2.52	-0.63	61.3	59.5		58.9	66.1	...
Ca I	5590.12	2.52	-0.65	59.7	58.7		59.4	64.1	...
Ca I	6161.28	2.52	-1.33	26.9	25.8	61.5	25.1	28.7	...
Ca I	6166.43	2.52	-1.19	34.3	32.1	72.1	32.0	36.3	...
Ca I	6169.03	2.52	-0.85	55.3	51.8	102.0	55.7	58.5	...
Ca I	6169.55	2.52	-0.58	74.0	69.1		74.4		...
Ti I	4820.40	1.50	-0.34	17.2	15.4	45.5	14.9	18.7	...
Ti I	4913.61	1.87	0.18	23.4	21.1	55.3	19.9	25.4	...
Ti I	4999.50	0.83	0.27	77.4	75.2		76.3	81.0	...
Ti I	5016.16	0.85	-0.55	36.0	32.4		33.0	39.6	...
Ti I	5022.86	0.83	-0.41	44.0	40.0		42.1	46.4	...
Ti I	5024.84	0.82	-0.55	36.9	33.9		35.0	41.2	...
Ti I	5039.95	0.02	-1.12	48.5	45.0		46.8	52.3	...
Ti I	5147.47	0.00	-1.97	13.7	11.3	39.0	13.4	16.6	...
Ti I	5192.97	0.02	-0.99	56.2	51.9		54.1	58.8	...
Ti I	5210.38	0.05	-0.85	62.3	57.4		61.5		...
Ti I	5866.41	1.07	-0.78	18.9	16.0	52.3	15.7	21.5	...
Ti I	6258.10	1.44	-0.34	22.0	19.7	50.9	20.0	24.9	...
Ti I	6258.70	1.46	-0.19	27.7	24.4		24.4	30.6	...
Ti I	6261.10	1.43	-0.46	18.6	15.9	49.1	16.4	21.0	...
Cr I	4801.02	3.12	-0.19	14.3	12.6	52.0	15.3	14.5	...
Cr I	4936.33	3.11	-0.32	11.6	10.2	46.4	11.7	13.1	...
Cr I	5296.69	0.98	-1.52	47.0	43.8		53.3	51.7	...
Cr I	5300.74	0.98	-2.22	16.2	14.3		20.2	19.2	...
Cr I	5329.14	2.91	-0.17	22.9	20.9		24.5	23.7	...
Cr I	5345.80	1.00	-1.08	67.3	66.6		73.1	74.0	...
Cr I	5348.32	1.00	-1.42	51.3	48.7		57.3	56.0	...
Mn I	4783.4	2.30	-0.04	70.0	67.7		79.4	77.4	...
Mn I	4823.5	2.32	0.05	71.7	68.5		77.6	78.4	...
Mn I	6013.5	3.07	-0.42	13.4	12.9	88.3	15.1	15.3	...

**Table 3.** continued

Element	wavelength [Å]	exc.pot. [eV]	$\log(gf)^a$	HD 22879 EW [mÅ]	HD 76932 EW [mÅ]	solar flux EW [mÅ]	CD -45 3283 EW [mÅ]	G 159-50 EW [mÅ]	etc.
Mn I	6016.7	3.07	-0.25	19.6	18.0	97.9	21.0	21.2	...
Mn I	6021.8	3.07	-0.10	24.5	23.0	102.4	27.0	27.5	...
Fe I	4788.76	3.24	-1.74	28.9	26.2	71.4	30.6	29.2	...
Fe I	4800.64	4.14	-1.10	20.6	19.3		22.3	21.4	...
Fe I	4924.77	2.28	-2.17	54.3	51.2		59.2	55.5	...
Fe I	4939.68	0.86	-3.32	65.6	62.6				...
Fe I	4950.10	3.42	-1.56	30.6	28.6		34.2	32.0	...
Fe I	4962.57	4.18	-1.18	17.1	15.4	59.7	17.6	16.4	...
Fe I	4973.09	3.96	-0.77	44.2	41.7		47.2	45.9	...
Fe I	5044.21	2.85	-2.07	32.5	29.8		36.2	33.8	...
Fe I	5054.67	3.64	-2.04	8.6	7.4	44.1	9.0	10.5	...
Fe I	5067.14	4.22	-0.86	27.7	26.1		31.2	28.9	...
Fe I	5074.74	4.22	-0.13	67.6	65.5		75.0	71.7	...
Fe I	5090.77	4.26	-0.49	45.1	42.0		48.6	46.2	...
Fe I	5109.65	4.30	-0.73	30.5	28.5	84.7	33.3	31.1	...
Fe I	5126.19	4.26	-0.85	27.3	23.8		28.1	27.7	...
Fe I	5127.36	0.91	-3.33	62.6	61.7		67.7	66.5	...
Fe I	5131.47	2.22	-2.46	43.2	39.8		46.1	45.3	...
Fe I	5141.74	2.42	-2.23	45.4	41.7		49.1	48.0	...
Fe I	5145.09	2.20	-3.15	15.5	13.2		18.8	18.7	...
Fe I	5159.05	4.28	-0.81	27.9	25.8		29.3	28.6	...
Fe I	5187.91	4.14	-1.24	16.7	15.1		17.8	16.7	...
Fe I	5198.71	2.22	-2.14	58.6	58.0		66.3	61.1	...
Fe I	5225.52	0.11	-4.75	33.7	30.4	75.0	41.5	37.6	...
Fe I	5228.37	4.22	-1.05	19.9	18.7		20.2	21.0	...
Fe I	5242.49	3.63	-0.99	47.9	45.5		50.3	48.7	...
Fe I	5243.77	4.26	-0.99	20.8	19.6	65.6	22.0	21.6	...
Fe I	5247.05	0.09	-4.91	27.4	24.0		34.1	32.2	...
Fe I	5250.21	0.12	-4.90	26.9	23.4		33.7	31.4	...
Fe I	5250.64	2.20	-2.09	61.9	61.7		68.1	67.0	...
Fe I	5253.46	3.28	-1.65	33.2	31.0		38.5	35.4	...
Fe I	5263.30	3.26	-0.97	73.2	70.5				...
Fe I	5281.79	3.04	-0.94	87.6	83.4		101.5		...
Fe I	5288.52	3.69	-1.59	19.0	17.3	57.7	19.7	19.5	...
Fe I	5307.36	1.61	-2.97	47.6	45.7		51.9	49.8	...
Fe I	5321.10	4.43	-1.26	9.0	8.4	40.9	10.0	9.3	...
Fe I	5322.04	2.28	-2.92	20.4	18.1	64.6	24.2	22.4	...
Fe I	5339.93	3.26	-0.80	86.4	79.5				...
Fe I	5364.87	4.44	0.11	73.4	68.2				...
Fe I	5365.40	3.57	-1.25	39.2	36.4		41.3	39.7	...
Fe I	5367.47	4.41	0.19	79.7	75.5				...
Fe I	5373.70	4.47	-0.77	22.1	20.6	67.9	24.4	22.4	...
Fe I	5379.57	3.69	-1.53	21.0	19.3	65.2	22.4	22.0	...
Fe I	5389.48	4.41	-0.45	39.9	37.4		43.6	40.6	...
Fe I	5393.17	3.24	-0.80	87.5	79.9		104.5		...
Fe I	5398.28	4.44	-0.60	30.9	28.5	78.1	32.6	30.5	...
Fe I	5409.13	4.37	-1.06	15.1	14.5	54.9	16.7	16.7	...
Fe I	5415.20	4.39	0.42	97.5	92.2				...
Fe I	5432.95	4.44	-0.63	27.9	28.9		27.8	26.8	...
Fe I	5445.04	4.39	0.00	67.1	64.7		74.8	70.2	...
Fe I	5473.90	4.15	-0.78	35.3	33.1		38.5	36.1	...
Fe I	5501.47	0.96	-3.06	74.8	73.5		80.7	78.1	...
Fe I	5543.93	4.22	-1.03	21.1	19.6	67.5	22.6	22.0	...
Fe I	5554.89	4.55	-0.36	38.1	35.8		41.3	39.3	...
Fe I	5560.21	4.43	-1.04	14.4	13.3	54.5	15.4	14.8	...
Fe I	5567.39	2.61	-2.66	18.1	17.1		21.7	20.6	...
Fe I	5569.62	3.42	-0.63	89.0	82.6				...
Fe I	5576.09	3.43	-0.94	67.2	63.6		75.0		...

**Table 3.** continued

Element	wavelength [Å]	exc.pot. [eV]	$\log(gf)^a$	HD 22879 EW [mÅ]	HD 76932 EW [mÅ]	solar flux EW [mÅ]	CD -45 3283 EW [mÅ]	G 159-50 EW [mÅ]	etc.
Fe I	5618.63	4.21	-1.27	13.6	12.9	50.3	14.3	13.9	...
Fe I	5624.55	3.42	-0.82	76.2	70.6				...
Fe I	5633.94	4.99	-0.23	24.0	22.0		25.3	23.6	...
Fe I	5638.26	4.22	-0.78	32.1	30.3	83.7	35.0	33.9	...
Fe I	5679.02	4.65	-0.71	17.6	17.7	63.1	19.4	18.4	...
Fe I	5686.53	4.55	-0.57	28.2	26.6		31.2	28.4	...
Fe I	5701.55	2.56	-2.21	40.3	38.3	86.2	45.7	43.4	...
Fe I	5717.83	4.28	-1.01	19.5	19.6		22.5	20.4	...
Fe I	5731.76	4.26	-1.11	17.3	16.0	60.7	20.6	18.0	...
Fe I	5852.22	4.55	-1.15	9.5	8.7	44.1	9.5	9.1	...
Fe I	5856.09	4.29	-1.52	6.9	6.8	33.2	7.6	7.0	...
Fe I	5859.59	4.55	-0.58	27.7	26.5		30.3	28.1	...
Fe I	6003.01	3.88	-1.10	33.5	31.9		38.2	35.5	...
Fe I	6024.06	4.55	-0.02	59.0	53.8		68.0	59.1	...
Fe I	6027.05	4.07	-1.13	24.1	21.9	67.0	28.0	24.9	...
Fe I	6079.01	4.65	-0.99	10.8	10.1	49.0	12.6	10.1	...
Fe I	6082.71	2.22	-3.58	7.0	5.7	35.0	7.6	8.3	...
Fe I	6151.61	2.18	-3.31	12.7	11.4	49.9	15.2	15.7	...
Fe I	6157.72	4.07	-1.20	21.1	19.8	61.9	23.5	21.3	...
Fe I	6165.35	4.14	-1.49	10.6	10.1	44.3		9.9	...
Fe I	6173.33	2.22	-2.88	25.5	24.3	71.2	30.5	29.5	...
Fe I	6180.20	2.73	-2.70	14.3	13.4	55.3	18.6	17.5	...
Fe I	6200.31	2.61	-2.43	28.8	26.6	76.4	34.3	31.6	...
Fe I	6213.43	2.22	-2.55	40.9	39.1	86.2	46.1	45.2	...
Fe I	6219.28	2.20	-2.43	48.7	45.8	96.7	54.0	51.6	...
Fe I	6246.32	3.60	-0.87	63.9	58.9		74.4	65.7	...
Fe I	6252.55	2.40	-1.72	75.5	73.2	128.5	82.1	82.2	...
Fe I	6265.13	2.18	-2.52	45.3	42.5	90.9	49.9	47.5	...
Fe I	6335.33	2.20	-2.26	57.3	55.2		65.2	62.6	...
Fe I	6336.82	3.69	-0.93	54.6	51.9		64.5	56.7	...
Fe I	6355.03	2.84	-2.31	24.5	22.6		29.4	26.1	...
Fe I	6358.68	0.86	-4.24	26.3	22.9	83.9	32.8	30.3	...
Fe I	6393.60	2.43	-1.60	80.9	78.2		91.2	88.7	...
Fe I	6411.65	3.65	-0.69	73.1	68.1				...
Fe I	6421.35	2.28	-2.02	67.3	63.8		75.2	70.2	...
Fe I	6430.85	2.18	-2.01	71.3	69.7		78.6	75.6	...
Fe II	4993.34	2.81	-3.73	15.2	15.9	41.4	11.2	12.4	...
Fe II	5132.66	2.81	-4.17	6.4	6.7	25.6	4.4	6.1	...
Fe II	5197.57	3.23	-2.33	56.0	60.8		47.0	48.8	...
Fe II	5234.62	3.22	-2.29	58.2	63.6	89.1	49.8	51.7	...
Fe II	5264.80	3.23	-3.15	20.8	23.2	45.8	14.7	15.8	...
Fe II	5284.10	2.89	-3.20	32.4	34.5		23.4	26.2	...
Fe II	5325.55	3.22	-3.25	18.2	19.6	41.4	13.0	13.4	...
Fe II	5414.07	3.22	-3.63	8.8	9.5	27.8	6.0	6.0	...
Fe II	5425.25	3.20	-3.31	17.1	18.1	44.0	11.5	12.5	...
Fe II	5534.84	3.24	-2.88	32.7	35.4	59.1	25.3	26.6	...
Fe II	6084.09	3.20	-3.83	6.2	7.0	20.7	3.7	3.8	...
Fe II	6149.24	3.89	-2.75	14.7	15.8	36.4	10.1	9.7	...
Fe II	6238.38	3.89	-2.63	18.2	19.8	43.8	12.2	12.5	...
Fe II	6247.55	3.89	-2.38	27.1	29.6	52.5	19.8	21.2	...
Fe II	6416.92	3.89	-2.75	15.1	16.2	40.4	10.2	11.9	...
Fe II	6432.67	2.89	-3.65	16.4	18.1	41.0	11.5	13.1	...
Ni I	4806.98	3.68	-0.60	21.5	20.2		17.4	20.6	...
Ni I	4829.02	3.54	-0.33	40.1	38.0		35.3	40.3	...
Ni I	4831.17	3.61	-0.38	34.1	31.9	77.6	28.3	34.1	...
Ni I	4904.41	3.54	-0.19	47.8	45.2		43.3	47.8	...
Ni I	4913.97	3.74	-0.62	18.4	18.1	60.0	15.0	19.1	...

**Table 3.** continued

Element	wavelength [Å]	exc.pot. [eV]	$\log(gf)^a$	HD 22879 <i>EW</i> [mÅ]	HD 76932 <i>EW</i> [mÅ]	solar flux <i>EW</i> [mÅ]	CD −45 3283 <i>EW</i> [mÅ]	G 159-50 <i>EW</i> [mÅ]	etc.
Ni I	4935.82	3.94	−0.31	23.3	21.7	64.5	19.2	23.3	...
Ni I	4937.34	3.61	−0.38	35.0	32.4		29.4	34.7	...
Ni I	4953.20	3.74	−0.61	19.7	17.6	60.0		19.2	...
Ni I	4998.22	3.61	−0.76	18.2	17.0		14.3	18.1	...
Ni I	5010.93	3.63	−0.85	15.2	13.9	51.7	10.8	14.4	...
Ni I	5035.36	3.63	0.12	59.3	60.0		56.0	60.7	...
Ni I	5081.11	3.85	0.22	54.0	52.5		50.2	55.3	...
Ni I	5082.34	3.66	−0.55	24.7	23.5	75.4	20.4	25.5	...
Ni I	5084.09	3.68	−0.04	48.8	47.7		43.1	49.3	...
Ni I	5099.93	3.68	−0.18	40.7	40.3		35.7	41.0	...
Ni I	5102.96	1.68	−2.83	12.3	11.6		11.1	14.1	...
Ni I	5115.39	3.83	−0.14	35.9	34.3		31.4	35.8	...
Ni I	5155.12	3.90	−0.63	14.3	13.0	53.1	11.5	14.6	...
Ni I	5155.76	3.90	−0.11	34.2	32.8		30.0	34.8	...
Ni I	5176.55	3.90	−0.46	19.8	17.9	59.7	14.4	19.4	...
Ni I	5578.72	1.68	−2.74	15.9	14.4		14.0	17.4	...
Ni I	5587.86	1.93	−2.41	18.2	17.0		17.8	19.8	...
Ni I	5682.20	4.10	−0.43	15.0	13.8	53.4	11.0	14.5	...
Ni I	6086.28	4.26	−0.49	10.3	9.3	44.3	8.3	10.8	...
Ni I	6108.12	1.68	−2.61	20.8	19.8	67.5	19.5	25.0	...
Ni I	6175.36	4.09	−0.51	13.3	12.8	49.2	10.6	13.6	...
Ni I	6176.81	4.09	−0.31	19.5	18.6	67.9	16.6	20.8	...
Cu I	5105.5	1.39	−1.58	31.3	25.7	95.9	18.2	32.4	...
Cu I	5218.2	3.82	0.36	13.7	12.2	56.5	6.8	12.1	...
Cu I	5782.1	1.64	−1.78						...
Zn I	4722.15	4.03	−0.50			70.8			...
Zn I	4810.53	4.08	−0.31	48.8	48.5	82.8	37.7	45.7	...
Y II	4883.68	1.08	0.01	39.0	40.3	63.9	25.0	35.5	...
Y II	5087.42	1.08	−0.28	26.2	27.8	51.0	14.4	23.9	...
Ba II	5853.68	0.60	−0.94	38.9	41.9	70.2	32.9	39.6	...
Ba II	6141.72	0.70	0.06	84.2	87.7	132.5	81.7	87.5	...

<sup>a</sup> The large majority of  $gf$ -values are determined from UVES spectra of the two standard stars, HD 22879 and HD 76932, as described in Sect. 2.1. For three lines that are only available in the FIES spectra (Mg I 4730.0, Cu I 5782.1, and Zn I 4722.2), the  $gf$ -value is determined so that for the sample of FIES stars, the mean elemental abundance derived from the line agrees with the mean abundance derived from the other lines of the element.